Volume 18
Number 7
7 April 2025
Pages 3049–3420

Energy & Environmental Science

rsc.li/ees

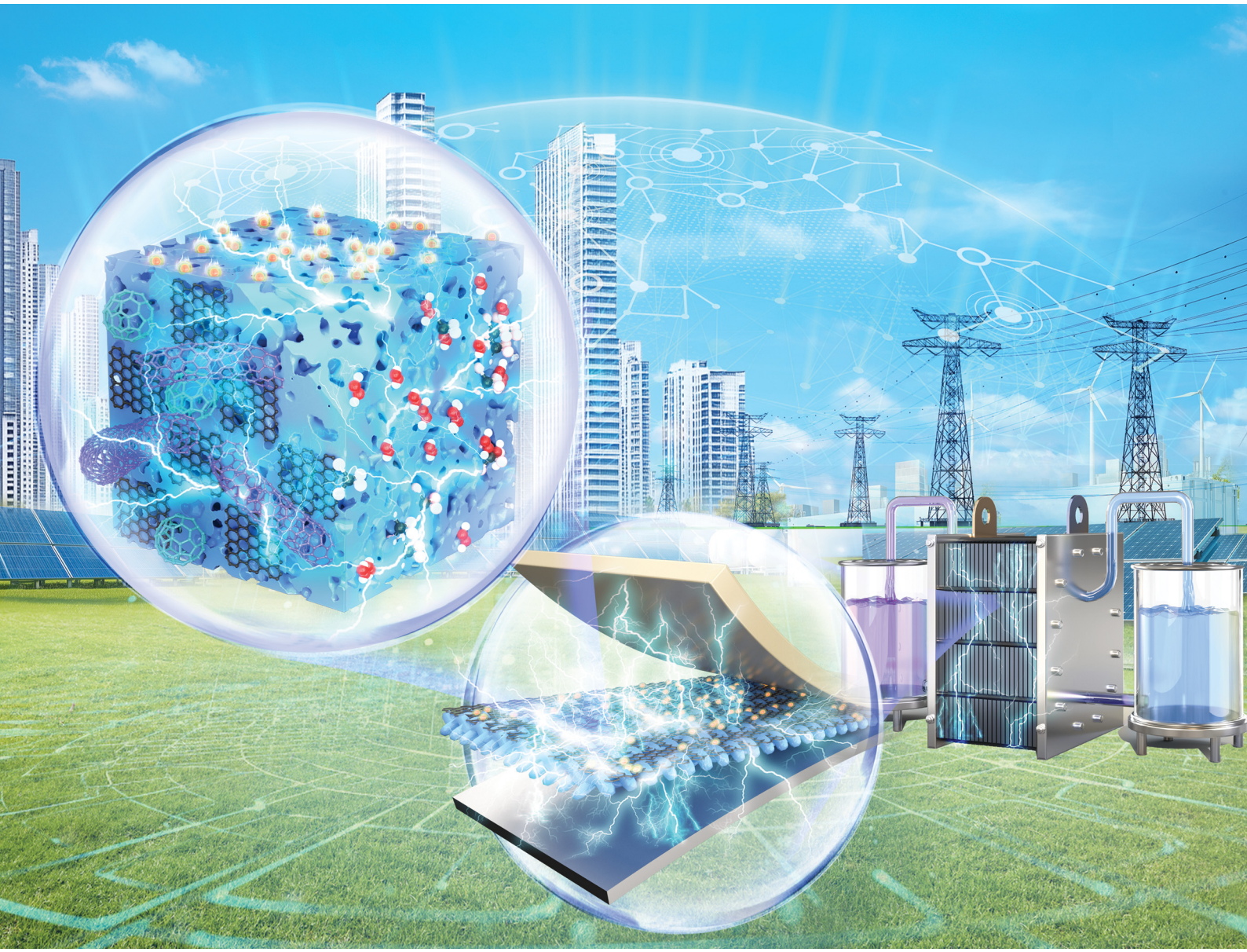

ISSN 1754-5706

ROYAL SOCIETY OF CHEMISTRY

REVIEW ARTICLE

Meisheng Han, Tianshou Zhao *et al.*
Strategies for improving the design of porous fiber felt electrodes for all-vanadium redox flow batteries from macro and micro perspectives

Energy & Environmental Science

ROYAL SOCIETY OF CHEMISTRY

REVIEW

View Article Online
View Journal | View Issue

Cite this: *Energy Environ. Sci.*, 2025, **18**, 3085

Strategies for improving the design of porous fiber felt electrodes for all-vanadium redox flow batteries from macro and micro perspectives

Hengyuan Hu,[ab] Meisheng Han,*[ab] Jie Liu,[ab] Kunxiong Zheng,[ab] Zhiyu Zou,[ab] Yongbiao Mu,[ab] Fenghua Yu,[ab] Wenjia Li,[ab] Lei Wei,[ab] Lin Zeng[ab] and Tianshou Zhao*[ab]

Received 25th November 2024,
Accepted 18th February 2025

DOI: 10.1039/d4ee05556j

rsc.li/ees

All-vanadium redox flow batteries (VRFBs) have emerged as a research hotspot and a future direction of massive energy storage systems due to their advantages of intrinsic safety, long-duration energy storage, long cycle life, and no geographical limitations. However, the challenges around cost constrain the commercial development of flow batteries. Increasing the power density and energy efficiency of the flow batteries is key to breaking through the cost bottlenecks, which is closely related to porous fiber felt electrodes (PFFEs), in which redox reactions take place. Therefore, it is essential to summarize advanced strategies for improving the design of electrodes, which are conducive to the further expansion of low-cost and high-performing flow batteries. This paper reviews the growth rate and market size of the flow batteries, and summarizes the latest research progress in the improvement strategies of PFFEs from macro and micro perspectives, including structure design based on the data model, intrinsic treatment, and introduction of catalysts. Finally, this review summarizes the practicability of the above strategies and the prospective modification approaches, and looks forward to the future optimization directions of PFFEs, such as exploring the modification mechanisms using advanced *in situ* characterization techniques, introducing high-entropy catalysts, adopting new preparation technologies, and incorporating artificial intelligence. The review offers the optimization strategies of PFFEs for flow batteries and bridges the gap between the academic literature and industrial manufacturing.

Broader context

High-efficiency and long-duration energy storage technology is vital for stabilizing the grid and integrating renewable sources like solar and wind energy. All-vanadium redox flow batteries (VRFBs) are ideal for large-scale and long-duration energy storage due to their intrinsic safety, long life, and scalability. However, their high cost limits commercial adoption. Reducing the cost depends on improving power density and energy efficiency, with porous fiber felt electrodes (PFFEs) playing a key role. A systematic review of optimization strategies for the design of PFFEs is essential to bridge the gap between research and industrial application, accelerating the adoption of VRFB technology. In this context, this review explores various modification strategies for PFFEs from macroscopic and microscopic perspectives. It covers techniques such as multi-level structural designs, intrinsic treatments, heteroatom doping, and catalyst introduction. Macroscopic strategies aim to improve electrolyte flow and reaction efficiency, while microscopic optimization focuses on enhancing conductivity and activating reaction sites. The review also summarizes the practicability of the above strategies and the prospective modification approaches. Besides, the review proposes future research directions of PFFEs, including investigating electrode–electrolyte interfacial mechanisms using *in situ* characterization techniques, introducing high-entropy catalysts, adopting new preparation technologies, and incorporating artificial intelligence. This comprehensive review provides crucial insights that can drive VRFB technologies forward and is expected to have a profound impact on the large-scale deployment of energy storage solutions in the future.

1. Introduction

Excessive reliance on fossil energy has led to irreversible environmental pollution and energy depletion, triggering a research frenzy in renewable energy such as solar energy, wind energy, *etc.* Despite the rapid development of photovoltaics and

[a] *Shenzhen Key Laboratory of Advanced Energy Storage, Department of Mechanical and Energy Engineering, Southern University of Science and Technology, Shenzhen, 518055, China. E-mail: hanms@sustech.edu.cn, zhaots@sustech.edu.cn*
[b] *SUSTech Energy Institute for Carbon Neutrality, Southern University of Science and Technology, Shenzhen, 518055, China*

wind turbines over the past decade, and the rapid decline in the cost of photovoltaic and wind power, there is a huge difference between installed capacity and grid-connected electricity. This is because solar energy and wind energy have intermittent, decentralized, and unstable characteristics. The most effective way to overcome the shortcomings of renewable energy is to develop energy storage technology. As an important and the most mature energy storage device, lithium-ion batteries (LIBs) have the characteristics of high energy density and fast response, which make them very suitable for medium- and short-duration energy storage.[1] Nonetheless, the potential safety hazards posed by LIBs during use and the inability to achieve long-duration energy storage prompt researchers to explore new, intrinsically safe, and long-duration energy storage technologies. Long-duration energy storage technology can not only effectively solve the intermittent problem of renewable energy power generation but also assist in building a new power system dominated by new energy, which is of great significance to the global energy layout. Notably, the Global Long-Duration Energy Storage Council released a report during the 29th United Nations Climate Change Conference, stating that long-duration energy storage is the key to achieving the net-zero emission target. By 2040, the global deployment scale of long-duration energy storage systems is expected to increase to 8 TW, which is 50 times the current scale. Therefore, it is crucial to develop intrinsic safe and long-duration energy storage devices.

As a new type of long-duration energy storage device, water-based redox flow batteries have received favor from researchers due to their intrinsically safe, flexible duration, and wide application scenarios. Currently, the all-vanadium redox flow batteries (VRFBs) represent a type of the widely used flow batteries in business, which is attributed to their advantages such as no toxic by-products, environmental friendliness, high safety, and high energy efficiency (EE).[2] Particularly, compared to rival LIBs, VRFBs have the core advantages of intrinsic safety, long cycling life, long-duration energy storage, and environmental friendliness. First, the use of water-based electrolytes in VRFBs determines their intrinsic safety. The safety of energy-storage batteries is an important guarantee for their rapid development. For LIBs, internal or external shorts would raise the internal temperature of the battery and thus accelerate exothermic reactions at both the anode and cathode, triggering combustion of organic electrolytes and thus leading to thermal runaway. Excitingly, these mechanisms do not occur in VRFBs due to the decoupling of capacity and power and the usage of water-based electrolytes, which can effectively prevent the occurrence of the troublesome thermal runaway seen in LIBs, thus enhancing safety and stability. Second, VRFBs have no phase change during charging and discharging and can be deeply charged and discharged, implying a long cycle life and low self-discharge probability. Third, compared to LIBs (a short- and medium-duration energy-storage technology), the decoupling of capacity and power endows VRFBs with the characteristic of long-duration energy storage, which is more effective at addressing the intermittent power output of solar and wind power, favoring increasing the proportion of new energy generation. Finally, the electrolytes of VRFBs can be recycled, significantly reducing resource waste and exhibiting high environmental protection. Despite their advantages, VRFBs continue to encounter cost-related challenges. Based on partial data, the cost of VRFBs is approximately 2.6 CNY per W h, whereas the average cost of LIBs is around 1.2 CNY per W h, only roughly 46% of VRFBs. More importantly, LIBs currently account for $\sim$97% of the battery energy storage market size, while VRFBs account for less than 0.6%, even lower than that of lead–acid batteries ($\sim$1.0%, a low-cost and technologically mature aqueous battery for energy storage). The key factor limiting the large-scale development of VRFBs is their high cost. It can be predicted that once the cost bottleneck is broken through, VRFBs can achieve rapid and large-scale development in the next 10–20 years due to the characteristics of their intrinsic safety, long cycle life as well as long-duration energy storage, and their market share in the field of battery energy storage may reach 30–40% by 2040. Hence, decreasing VRFBs' cost is urgently needed and is the top priority for future development.

Enhancing the EE and power density of VRFBs is crucial for overcoming the cost limitations. As shown in Fig. 1, VRFBs are primarily composed of battery stacks, positive/negative electrolytes, and battery management systems, accounting for 24%, 58%, and 18% of the VRFB cost, respectively, calculated based on a 4 h energy-storage duration.[3] Among them, the battery stack provides a place for electrochemical reactions, and is the core component of the energy storage system to realize the mutual conversion of electrical energy and chemical energy.[4] The battery stack is mainly composed of membranes, electrodes, bipolar plates, current collectors, and electrode frames, which have a great impact on the cost, power, cycle life, efficiency, and maintenance performance of the energy storage system. Specifically, the cost of VRFBs is closely related to their own EE and power density. On the one hand, increasing EE and power density can effectively reduce the usage amount of key components and volume of the battery stack. When the current density of the battery increases from 180 mA cm^{-2} to 400 mA cm^{-2}, under the same battery capacity, the areas of the electrodes, membranes, and bipolar plates will all be reduced to 45% of the original. Taking a 16 kW stack as an example, when the rated current density increases from 180 to 400 mA cm^{-2} and the prerequisite is that EE is above 80%, the size of the stack can be reduced from 1026 $\times$ 650 $\times$ 450 mm to 640 $\times$ 560 $\times$ 510 mm (data from the research in our team). The obvious reduced volume can greatly decrease the battery stack cost. On the other hand, the improvement of EE and power density also helps to improve the electrolyte utilization, thus extending the energy-storage duration of VRFBs. The improvement of electrolyte utilization can reduce the amount of electrolyte used, thereby lowering costs. Besides, the extension of energy-storage duration also can decrease cost. For example, when energy-storage duration is extended from 4 to 10 h, the system cost of VRFBs will be reduced by 30–40%. After multiple cost compressions, the cost of VRFBs may reach 1–1.5 CNY per W h

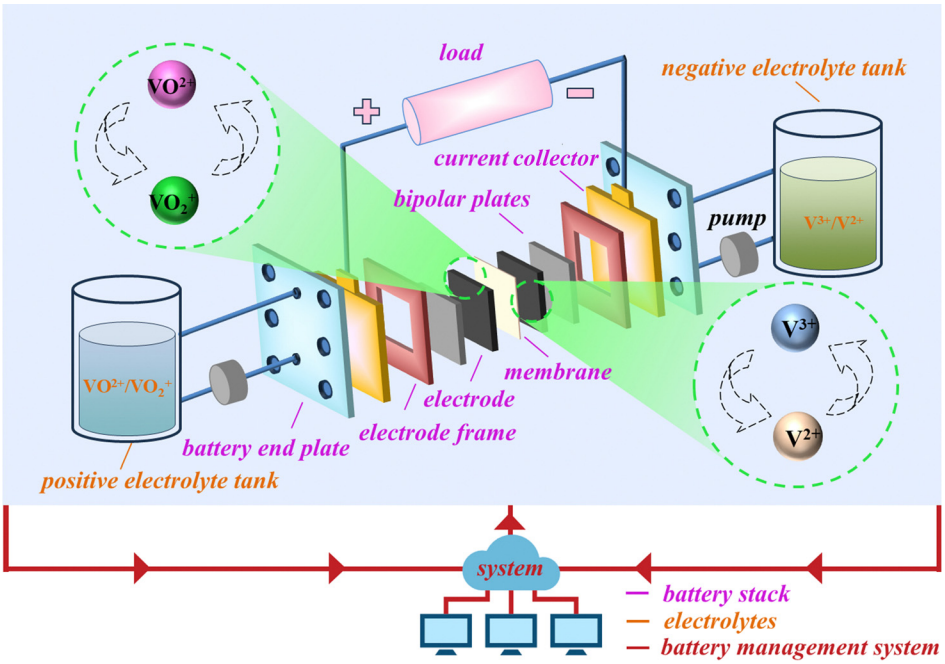

Fig. 1 Schematic diagram of the components of a flow battery.

within the next 10 years.[3] At that time, it will be on par with the cost of its competitor LIBs, which will greatly promote the large-scale development of VRFBs. Therefore, optimizing the performance of VRFBs is crucial. As an important component of the battery stack, porous fiber felt electrodes (PFFEs) are the key to determining EE and power density of the stack and even VRFBs. Electrodes mediate complex reaction processes involving macroscopic electrolyte flow, microscopic mass transport, and interfacial electrochemical reactions. At the microscopic level, ion transport is dependent on convection (determined by electrolyte flow rate), diffusion (driven by concentration gradients), and migration (driven by potential differences). At the electrode–electrolyte interfaces, ions undergo adsorption, electron transfer, and desorption. At the macroscopic level, owing to the optimal pore size distribution, the designed porous electrodes ensure the effective mass transfer of the electrolyte and the relatively uniform distribution of velocity and concentration, which in turn determine the polarization and mass transfer problems on the electrode surface.[5] The above transport and reaction processes make PFFEs become the key components of VRFBs. Therefore, modifying the performances of PFFEs has become an important strategy to achieve cost reduction and efficiency increase in VRFBs.

At present, the market of the commercial PFFEs is huge, with a rapid development momentum. The newly installed capacity of VRFBs is increasing year by year, and the global flow battery market size exceeds 10 billion. It is worth noting that the market size of VRFBs in the Asia-Pacific region accounts for 32% of the global market share in 2021, with China's market size occupying a major portion. According to predictions from the Askci Consulting Co., Ltd and EVTank, the market size of VRFBs in China in 2025 will be approximately 8 billion CNY, with the market size of electrode materials being approximately 1.101 billion CNY. To meet the huge market demand for PFFEs, leading domestic and international PFFE enterprises such as Liaoning Jingu, Shenyang Fulai, Jiangyou Runsheng, SGL Group, and Toray Industries have established large-scale PFFE production lines, aiming to mass-produce low-cost and high-quality PFFEs for VRFBs to obtain significant profits. Notably, although commercial PFFEs have been produced on a large scale, their low catalytic activity, few active centers, and slow reaction kinetics greatly limit the EE and power density of VRFBs, preventing them from meeting the market's long-duration and efficient energy storage needs for flow batteries.[6] Therefore, modifying and optimizing PFFEs are crucial. The main purpose of PFFE modification and optimization is to increase the specific surface area (SSA) of the materials, introduce active centers, and improve the hydrophilicity and catalytic efficiency of the materials, thereby enhancing the adsorption and catalytic performance of PFFEs for vanadium ions, reducing the polarization problem and improving the power density and EE of VRFBs.[7] This paper provides an overview of the modification strategies for the design of PFFEs from two aspects: macrostructure designs based on electrolyte flow and microstructure designs based on mass transfer coupled with interfacial electrochemical reaction, as shown in Fig. 2. Finally, this review summarizes the valuable modification strategies of PFFEs, and puts forward practical suggestions for the long-term development of PFFEs. PFFEs can be divided into carbon felt (CF) and graphite felt (GF) due to different heat treatment temperatures, of which GF has a higher heat treatment temperature (>2000 °C) than CF (~1000 °C). Consequently, GF has a higher degree of graphitization, higher electrical conductivity, and better mechanical properties than

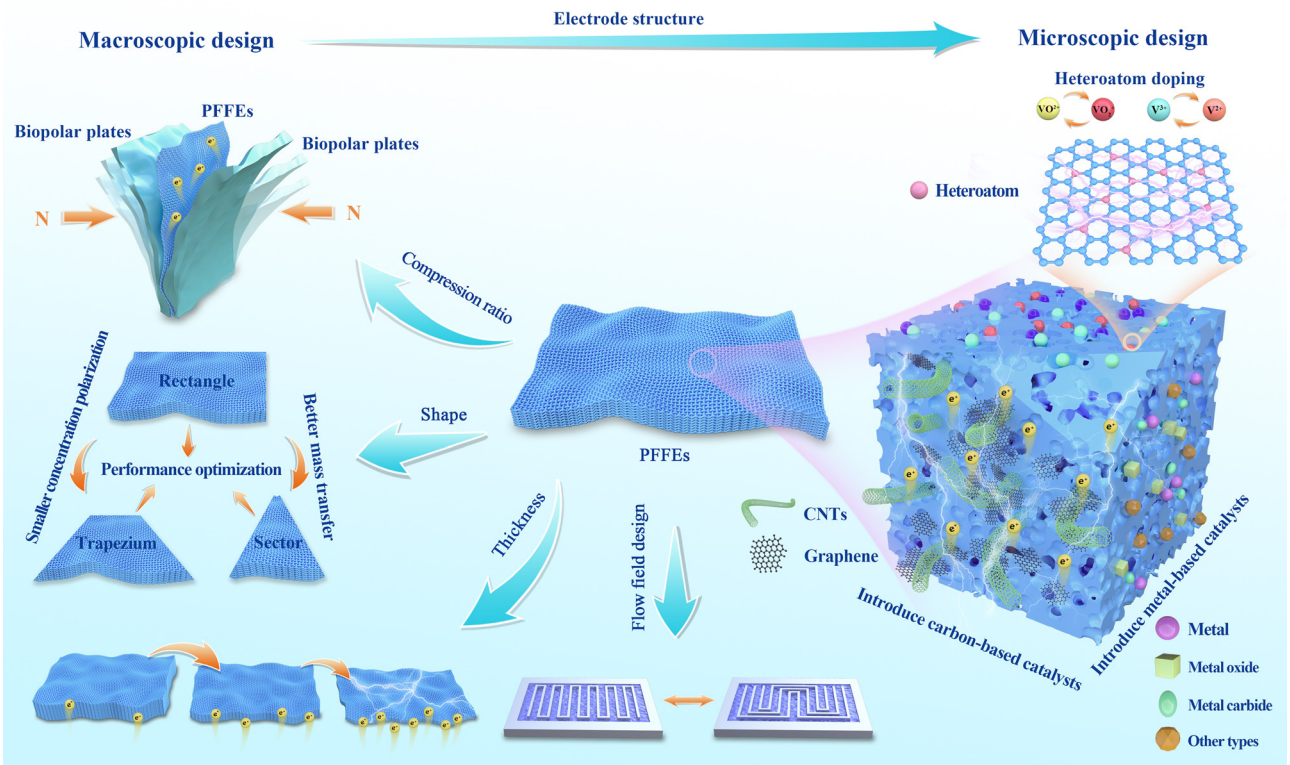

Fig. 2 Schematic diagram of PFFE modification strategies from macro to micro.

CF, endowing GF with a dominant demand in the current market. Nevertheless, GF and CF are both porous fiber felt products, which have similarities and versatility in modification strategies. Therefore, we do not give any additional distinction between CF and GF in subsequent discussions on the modification strategies.

2. Macroscopic design of the electrode structure

The macroscopic designs of the battery structure aim to design and optimize the deformation degree, external shape, and flow field structure of the electrode according to the specific needs and working conditions. These macroscopic designs are necessary, which are closely related to the polarization, mass transfer, and other problems existing in the flow batteries themselves. Specifically, there are usually three major types of polarization in VRFBs, namely ohmic polarization caused by the resistance of electrodes and electrolytes, concentration polarization caused by electrolyte diffusion and mass transfer, and electrochemical polarization caused by the electrochemical reactions occurring on the surface of PFFEs. These three types of polarization are closely related to a large difference in electrolyte flow rate, uneven concentration distribution, low mass transfer efficiency, and insufficient electrochemical reactions. The macroscopic designs of the electrode structure are an effective strategy to solve these bottlenecks. However, the macroscopic designs need to be carried out according to specific needs and working conditions, which determine that relying on the big data model to build the corresponding working conditions is the best way to design. Therefore, this section summarizes the macro designs of electrodes, such as compression ratio, shape, thickness, and flow field design, with the assistance of big data models, aiming to provide a reference for subsequent electrode research.

2.1 The compression ratio of the electrode

Typically, when assembling the PFFEs, the entire PFFEs are stacked with the separator and the graphite bipolar plate in sequence, then pressurized as a whole. While ensuring sealing, the PFFEs are compressed to reduce the contact resistance between the PFFEs and the graphite bipolar plate, and improve the electrolyte fluidity. However, this compression process may have problems such as increased liquid-phase mass transfer resistance, excessive compression affecting electrolyte flow rate, inconsistent compression rates leading to overcharging, and leakage in a sealed high-pressure environment. Therefore, it is necessary to explore the compression ratio of PFFEs in combination with model predictions to optimize the performance of electrode materials.

To explore the optimal compression ratio of PFFEs, Charvát *et al.* used a series of complex characterization techniques, including *ex situ* through-plane electrical conductivity measurement and comprehensive evaluation of single-cell performance, to regulate the compression effect of two different commercial CF electrodes, polyacrylonitrile-based electrodes and rayon

electrodes.[8] After testing, it was found that the area with a high electrode compression ratio has a small resistance, which can reduce the ohmic impedance and facilitate the rapid transfer of electrons. In contrast, the electrode with a low electrode compression ratio has high electrolyte permeability and a faster electrolyte flow rate, thereby reducing pump consumption. After weighing the charge–discharge load curve and pressure drop measurement data of the single cell, the researchers found that the optimal compression ratio of the polyacrylonitrile CF electrode is 30%, while the optimal compression ratio of the rayon CF electrode is 60%. At the optimal compression ratio, the total power loss caused by battery polarization and electrolyte pumping is evaluated as the minimum. It is worth noting that the optimal compression ratio of electrode materials can also be affected by the internal flow channels of the battery. Wang *et al.* tested the uneven electrode compression caused by the flow channel at different compression ratios and their impact on battery performance, and on this basis proposed an accurate model to study the influence of non-uniformly compressed electrodes on the flow and electrochemical performance of VRFBs with flow channels.[9] The presence of the flow channel results in different porosity and permeability in different regions. The results showed that during the electrode compression process, the spatial distribution of the flow channel affects the electrolyte flow rate, the local current density, and the distribution of overpotential. With the flow rate remaining unchanged, the increase in the compression ratio causes an increase in the pressure difference between adjacent flow channels and the volumetric flow rate also increases, thus enhancing mass transfer. When the

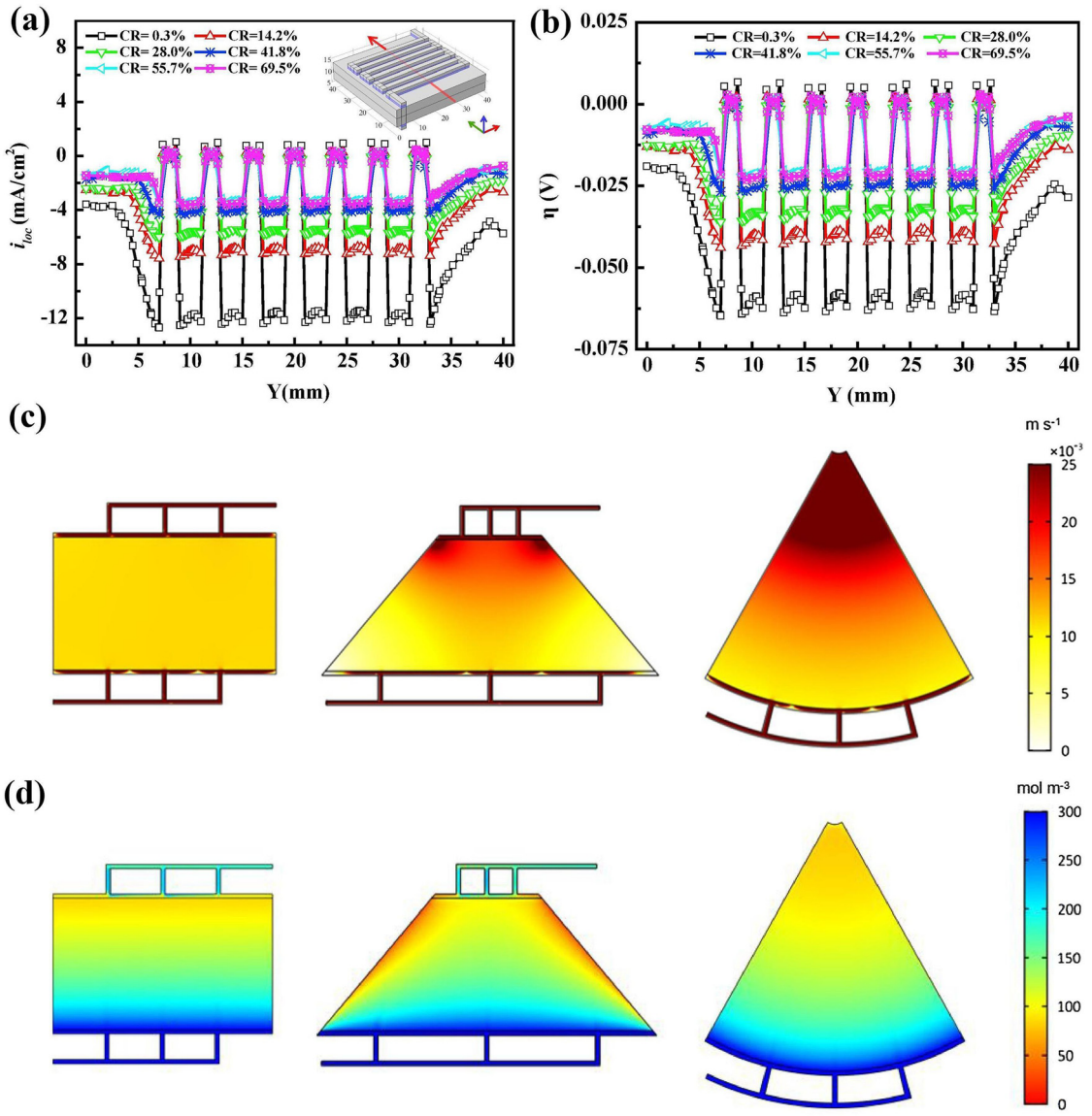

Fig. 3 Distributions of (a) current density and (b) overpotential (i = 40 mA cm^{-2}) under different electrode CRs.[9] Copyright (2018). Elsevier. The simulated contour plots of rectangular electrodes, trapezoidal electrodes and sector electrodes. (c) Velocity and (d) V^{3+} concentration.[10] Copyright (2019). Elsevier.

compression ratio is 55.7%, the distribution of active substances in the electrode is the most uniform, where the local current density and overpotential simulated by the model are the smallest, as shown in Fig. 3a and b. The non-uniform model proposed in this study can predict the influence of electrode compression and flow channels in VRFBs, providing an effective guidance for the design of VRFBs with compressed electrodes and flow channels.

2.2 The shape of the electrodes

Electrode shape is an often overlooked, but is an extremely important factor for improving the performance of flow batteries. The influence of the shape of the electrodes on the flow batteries is mainly reflected in the internal polarization and pumping consumption of the battery. The reason for this is that the change of electrode shape can significantly affect the electrolyte distribution, flow rate, and mass transfer correlation. However, it is difficult to study the concentration polarization and mass transfer problems through repeated experiments, and the establishment of data models for optimization has become an indispensable strategy. Building a data model and delving into the subtle link between electrode shape and battery performances is key to optimizing VRFB performance.

Conventional rectangular electrodes can cause a large electrolyte concentration difference between the inlet and outlet of the electrolyte, which in turn affects mass transfer and produces concentration polarization, especially at high current densities. Zheng *et al.* proposed to build a circular VRFB assembled with circular electrodes, and gradually reduced the electrode cross-sectional area from inlet to outlet.[11] Surprisingly, this circular electrode, with its decreasing cross-sectional area from inlet to outlet, improves the flow velocity and concentration difference of the electrolyte, thereby overcoming the disadvantages of concentration polarization and mass transfer of traditional rectangular electrodes. The assembled flow battery exhibits an EE of 83.31% at low flow rate, high current density, and low pump consumption. Not only circular electrodes, but also some trapezoidal and sector electrodes are also favored by researchers. Yue *et al.* proposed a trapezoidal electrode design to optimize the polarization and other problems in rectangular electrodes.[12] Owing to the trapezoidal electrodes' gradual reduction of the cross-sectional area from inlet to outlet, the flow velocity in the electrolyte gradually increases from inlet to outlet and peaks at outlet, which significantly improves electrolyte mass transfer and distribution. Compared with the above-mentioned circular electrode, the EE of the trapezoidal electrode is as high as 85.64% under the same working conditions, which is better than the performance of the circular electrode. With the help of a 3D model, Gurieff *et al.* designed a radial sector electrode structure to promote the flow rate and concentration distribution of the electrolyte based on shape dynamics.[10] Compared with the traditional rectangular and trapezoidal electrodes, the prepared sector electrode exhibits a higher electrolyte flow velocity and a more uniform concentration distribution, but there is a high pressure drop caused by rapid changes in the cross-sectional area, as shown in Fig. 3c and d.

Concentration polarization and limited mass transfer are headaches for flow batteries, which are closely related to the velocity and concentration distribution of the electrolyte. Designing electrodes with a decreasing inlet-to-outlet cross-section can effectively improve these problems because the design accelerates the flow rate of the electrolyte, promotes electrolyte distribution, and reduces pump consumption efficiency. However, some electrodes with higher curvature and greater design difficulty, such as circular electrodes and sector electrodes, are hard to quickly achieve the transition from laboratory research to industrial application. With the rapid development of 3D printing technology in terms of cost control and accuracy improvement, the related dilemma is expected to be significantly improved. Notably, the trapezoidal electrode is the most likely to be applied on a large scale in the future. Firstly, it can be processed and designed based on the existing rectangular electrodes, with low consumption of the process and cost. Secondly, compared with the traditional rectangular electrodes, the trapezoidal electrode has obvious advantages in mass transfer optimization and reduction of concentration polarization, which is an effective strategy to improve the performance of VRFBs. On the whole, trapezoidal electrodes are very promising electrode shapes, which can not only improve the disadvantages of traditional electrodes, but also reduce the problems of high voltage drop, which is in line with the needs of future commercial development.

2.3 The thickness of the electrode

Electrode thickness plays a crucial role in electrolyte distribution, cell polarization, conduction resistance, mass transfer efficiency, and power delivery in the power pump in VRFBs. On the one hand, a thinner electrode not only shortens the ion transport and electron transport distance, which is conducive to reducing ohmic polarization, but also reduces pumping power required, thereby improving overall efficiency.[13] However, a thinner electrode is unable to provide a large number of active sites and a wide reaction contact area for redox reactions in VRFBs, which leads to a relatively large electrochemical reaction polarization and restricts the efficiency of VRFBs. During the preparation process of PFFEs, rationally designing the thickness of the electrode can maximize the performance of the electrode. On the other hand, a thicker electrode will produce high ohmic losses caused by ohmic polarization, especially when working in the high power/current region of the battery, which will seriously restrict the power density of VRFBs. Therefore, it is crucial to explore the electrode thickness through model prediction and trade-off of multiple external factors.

Ali *et al.* established a three-dimensional (3D) numerical model for studying the electrode thickness size and porosity of VRFBs by combining the effects of electrode thickness and porosity, and electrolyte distribution and flow rate on VRFB performance.[14] The predicted results show that an increase in electrode thickness can enhance the distribution uniformity of

vanadium ion concentration, and the optimum thickness is 3 mm. At the same time, the decrease in electrode thickness and the increase in porosity can increase the pressure drop and pumping power, thereby providing the required electrolyte flow rate for VRFBs. In general, when the electrolyte flow rate is 10 ml min^{-1}, the battery with higher porosity and a thickness of 1 mm achieves the highest power efficiency of 96.8%, as shown in Fig. 4a–d. The 3D model proposed in this study has high applicability to VRFBs under low electrolyte flow conditions, and provides a certain reference for designing electrode thickness.

The choice of electrode thickness depends on the specific requirements, and the optimal thickness of the electrode varies according to different needs. At present, there are two main types of electrodes on the market, one is a thick electrode with a thickness of 1–6 mm.[16] Due to its high SSA, it is often used in traditional flow batteries. The second is a thin electrode with a thickness of 0.2–0.6 mm, which is often used in compact and miniaturized flow batteries.[17] To balance the relationship between electrode thickness, battery performance, and economic benefits, Muñoz-Perales *et al.* used the stacking method to change the electrode thickness to explore the optimal electrode thickness under two types of flow fields: flow-through flow fields (FTFF) and interdigitated flow fields (IDFF).[18] FFTF refers to a flow field with only one inlet and one outlet. IDFF refers to a flow field with multiple inlets and multiple outlets. Based on the established electrode material data model, it is found that the thicker electrode exhibits a lower voltage drop in FTFF, while the thinner electrode exhibits a higher mass transfer efficiency in IDFF. The electrochemical performance factors are comprehensively analyzed, and it is found that the electrodes with a thickness of 0.4–0.7 mm (stacked with 2 layers) may be the best configuration in terms of electrochemical performance under various flow field combinations. Furthermore, considering the electrochemical performance and related pressure loss, the thicker electrodes may be suitable for FTFF and the thinner electrodes may be suitable for IDFF.

Based on the data model, macroscopic control of electrode thickness is an efficient means to optimize the efficiency of VRFBs. Optimal electrode thickness is a combination of additional factors that need to be balanced. We believe that a thick electrode may be the best choice when there is a single-channel flow field and a full range of microscopic modifications to the electrode. However, thin electrodes may be the best choice when there is a multi-channel flow field, especially for stacks or flow batteries, which require miniaturization and low cost.

2.4 The flow field design of the electrode

Carefully designing PFFEs' flow field is key to improving VRFBs' performance. A well-designed flow field has many benefits, which can significantly boost the electrolyte flow rate, enhance mass transfer, and make electrolyte distribution more even in the battery. Moreover, it can prevent vanadium species from piling up on the electrode surface due to slow redox reactions, ensuring stable battery performance. Optimized flow field of PFFEs works excellent in reducing polarization. It can cut down concentration polarization from uneven diffusion and mismatched kinetics, and also lessen extra ohmic and electrochemical reaction polarization caused by poor electrolyte–electrode contact and incomplete reactions.[19]

Hao *et al.* used finite element analysis to adjust the flow field design of the CF electrode and achieved a significant increase in the power density of the vanadium flow battery. The researchers adopted parallel flow and cross-flow field designs for CF respectively, and revealed the positive effects of these two flow field designs in reducing CF pressure drop, in promoting the uniform distribution of reactants, and in increasing the flow rate, as shown in Fig. 4e–g.[15] According to the measured local mass transfer coefficient, the parallel flow field has a better improvement effect on concentration polarization than the cross-flow field design at 200 mA cm^{-2}. Further experimental verification shows that the CF with a parallel flow field has a VE of up to 78% at 200 mA cm^{-2} and the corresponding discharge capacity is also improved. To introduce the parallel flow field design into production, this experiment carried out dynamic modeling and simulation on a 32 kW industrial battery stack. The results show that the CF with parallel flow field design can also reach a system efficiency of 70% at 200 mA cm^{-2}, which has a positive guiding significance for the subsequent application of CF flow field design to actual production. In addition, our team also proposed to predict the electrolyte flow in VRFBs using a deep neural network (U-Net) based on the flow field characteristics, so as to accurately identify the dead zones, further increase the under-rib convection, and improve the flow field design.[20] Owing to the optimization of the flow field, the system efficiency of the battery at 200 mA cm^{-2} has been improved by 5.5%. Moreover, compared with the traditional numerical simulation, the U-Net-assisted prediction significantly reduces the computational time by 99.9%, greatly improving the efficiency. This new strategy of U-Net-assisted numerical simulation calculation is the key to optimizing the application of AI in flow field and even battery design. Therefore, we believe that applying some advanced machine learning or deep neural networks to assist in flow field design, especially the parallel flow field design, is a promising strategy at present.

3. Microscopic design of the electrode structure

In the energy conversion and storage of flow batteries, a large number of electrochemical reactions and microscopic mass transfer occur between the electrolyte and the electrode materials, which are mainly carried out through the contact, collision, and adsorption between the reactive ions and the electrode materials. Therefore, high-performance electrodes usually need to have a large number of active sites to provide a site for electrochemical reactions, which points out the directions for the microscopic design of electrode structures. This section summarizes the microscopic modification strategies of PFFEs,

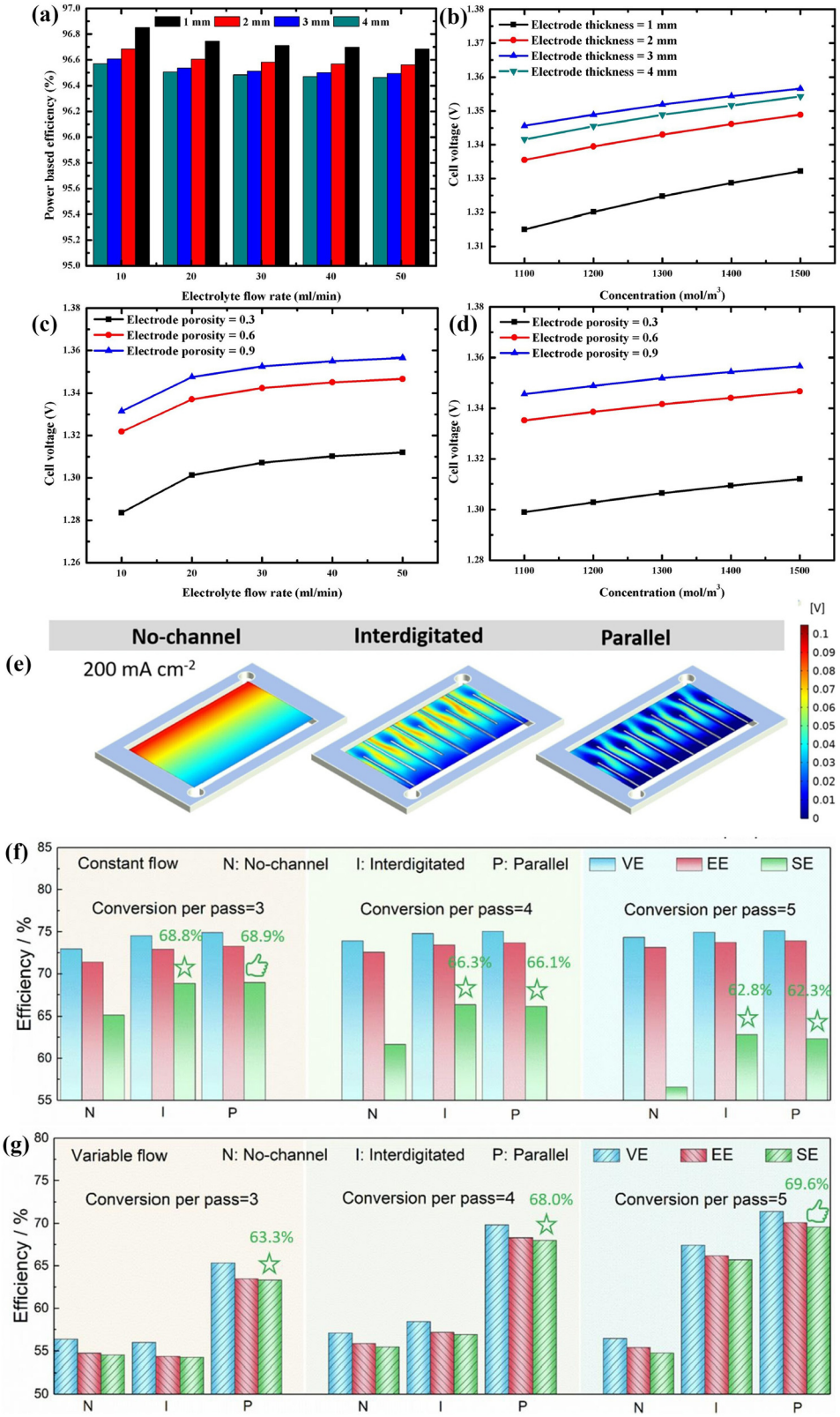

Fig. 4 (a) Power efficiency for different electrode thicknesses and electrolyte flow rates; numerical calculation of cell voltage (b) based on the concentration and electrode thickness, (c) based on the electrode porosity and electrolyte flow rate, and (d) based on the electrode porosity and concentration.[14] Copyright (2020). Elsevier. (e) Concentration polarization distribution on different felt designs at a current density of 200 mA cm^{-2}. 32 kW stack efficiency at varied conversion fractions per pass: (f) constant current mode and (g) variable flow mode.[15] Copyright (2022). Elsevier.

such as intrinsic treatment and introduction of catalysts, to provide new ideas for the subsequent research and development of electrodes.

3.1 Intrinsic treatment

Intrinsic treatment is a commonly used method in PFFE modification strategies. Its characteristics include a simple process and ease of operation, without introducing additional impurities. After intrinsic treatment, PFFEs remain intact, thereby ensuring relatively stable performance. In addition, intrinsic treatment can introduce functional groups and defects into the PFFEs, increasing the SSA and improving the hydrophilicity, local electronegativity, electrochemical catalytic activity, and reversibility of the PFFEs.[21] However, intrinsic treatment also has certain limitations, such as limited improvement of material properties.[22] This section reviews the two strategies of intrinsic processing: heteroatom doping and design of pores. In addition, this section also lists the relevant material properties of the two strategies in Table 1.

3.1.1 Heteroatom doping. Heteroatom doping mainly refers to heteroatoms entering the PFFE structures and undergoing redox reactions with PFFEs to form functional groups.[35] Heteroatom doping is widely used in the field of PFFE modification, which has a significant effect on improving the performance of VRFBs. The mechanisms of improving the role of PFFEs by doping heteroatoms are discussed as follows. (i) The doped heteroatoms will affect the electron distribution of PFFEs and change the charge density, which can reduce the adsorption/desorption reaction energy barrier of reactants and intermediates on the surface of PFFEs, thereby promoting the adsorption of vanadium ions.[36,37] (ii) The doped heteroatoms have different electronegativity compared to C atoms, which can effectively increase the active sites on the surface of PFFEs.[38] In addition, the lone electron pairs of heteroatoms can bond with the empty orbitals of vanadium ions, which not only improves the adsorption but also promotes the charge transfer. (iii) The doped heteroatoms can introduce a large number of defects and vacancies in PFFEs, and these structural defects are considered as active sites for improving the performance of PFFEs.[39,40] These structural defects can improve the SSA and electron transfer rate of PFFEs, and provide reaction sites for the redox reactions of vanadium ions.[41,42] (iv) The doped heteroatoms will undergo redox reactions with C atoms to form functional groups.[43] These functional groups can not only improve the hydrophilicity of PFFEs, promoting the adsorption of materials to vanadium ions, but also provide active sites to promote the redox reactions of vanadium ions.[44,45] Currently, heteroatoms commonly used for modification include elements such as O, N, B, S, P, *etc.*[46,47]

Zhang *et al.* took the copolymer of dopamine and polyethyleneimine as the precursor and nitrogen source of the electrode materials, and innovatively utilized the *in situ* interfacial copolymerization technique to deposit villous N-doped carbon onto CF electrodes.[23] Owing to the modification and optimization of N doping and the hierarchical interconnection structures of the materials, the assembled VRFBs exhibited a high EE of 73.6% at 300 mA cm^{-2}, and still maintained good stability and extremely low EE attenuation (energy attenuation per cycle is 0.006) after

Table 1 Performance comparison of different intrinsic modification strategies

Optimized strategies	Doped substances or improved topography		P_{max} (mW cm^{-2})	EE		R_{CT} (Ω)	R_{CT}[a] (Ω cm^2)	Ref.
				Cycle number	Current density (mA cm^{-2})		R_{CT}[b] (Ω cm^2)	
Heteroatom doping	Dopamine and polyethyleneimine	N	750.6	75.3%		0.06	—	23
				600	300			
	$(NH_4)_2SO_4$	N	350.9	87.34%		—		24
				25	80			
	CO_2	O	—	83.28%		3.30	—	25
				30	50			
	H_3BO_3	B	—	82.07		—		26
				2000	240			
	N_2, O_2	N, O	—	*ca.* 78%		26.7	—	27
				30	50			
	Silk protein	N, O	—	86.8%		—		28
				—	40			
	H_3BO_3, air	B, O	—	*ca.* 70%		—	1.6	29
				100	140		1.2	
	Ethylenediamine tetra	N, P	—	84%		—		30
				100	150			
	LiCl, KCl, $KClO_3$, NH_4Cl	N, O	—	75.9%		—	*ca.* 5	31
				140	260		*ca.* 5	
	Br_2	Br	—	86.8%		—		32
				—	50			
Design of pore	SSA and pore	540	*ca.* 75%		20		—	33
			200	120				
	SSA and pore	—	*ca.* 78%		—		0.068	34
			500	320			0.068	

[a] R_{CT} for VO^{2+}/VO_2^+. [b] R_{CT} for V^{2+}/V^{3+}.

600 cycles at 200 mA cm^{-2}. In-depth studies found that the improvement of the reaction kinetics of V^{2+}/V^{3+} is mainly due to the enhanced adsorption of V^{2+}/V^{3+} by the pyridine nitrogen formed by N doping, while the improvement of the reaction kinetics of VO^{2+}/VO_2^+ is mainly due to the doped N atoms significantly reducing the activation energy barrier of the corresponding reaction. Jiang *et al.* fabricated and tested VRFBs with the B-doped GF electrodes.[26] First-principles studies pointed out that the carbon surface of B doping has many active and stable reaction sites. After electrochemical testing, the VRFBs showed an EE of 87.40 and 82.52% at 160 and 240 mA cm^{-2}, respectively, and even showed an EE of 77.97 and 73.63% at 320 and 400 mA cm^{-2}, respectively, demonstrating their excellent performance based on the published literature. Even more excitingly, after 2000 cycles at 240 mA cm^{-2}, the VRFBs have only 0.028% and 0.0002% capacity and efficiency decay per cycle, respectively. Moreover, the degradation of battery performance caused by long-cycle testing can be recovered by refreshing the electrolyte. These results indicate that the stable and high-performance B-doped GF is an exciting electrode for VRFBs.

Additionally, compared to single-atom doping, multi-atom co-doping has a synergistic effect, resulting in a more comprehensive modification and optimization of PFFEs. Huang *et al.* introduced N and O atoms into CF electrodes through plasma treatment technology, fabricating N, O dual-doped electrodes (O-N-CF).[27] Compared to single-atom doping (O-CF and N-CF), the O-N-CF electrodes exhibit a better battery performance and a more outstanding VO^{2+}/VO_2^+ redox activity. This is mainly attributed to the numerous functional groups introduced by N and O doping, which provide the active sites for vanadium ion reactions, improve the material's conductivity, and enhance the performance of O-N-CF. Ammonium persulfate (APS) is rich in N atoms and S atoms. Researchers introduced N-containing and S-containing groups on CF electrodes through heat treatment with APS for use in VRFBs.[48] The CF electrodes treated with APS have a stable, oxygen-rich hydrophilic surface, significantly improving the overall performance of VRFBs. Zhang *et al.* prepared a N, P co-doped GF through a simple one-step activation method.[30] The synergy between N atoms and P atoms introduces a large number of active sites in GF electrodes. The corresponding VRFBs maintain an EE of 84% at 150 mA cm^{-2}. To enhance the doping efficiency and construct multi-dimensional defect engineering, a novel molten salt doping strategy is proposed. Jiang *et al.* used $KClO_3$ as the oxygen source and NH_4Cl as the nitrogen source, adopting a LiCl/KCl dual molten salt system to introduce N and O functional groups into GF electrodes, as shown in Fig. 5.[31] The molten salt system doping strategy not only uniformly incorporates heteroatoms into GF electrodes but also builds a porous structure deep within the GF electrodes. The modified GF electrodes possess abundant N and O groups, and a large number of micropores, significantly enhancing the SSA, wettability, and electronic structure properties of GF electrodes. Notably, the synergistic effect of N and O functional groups enables the CF electrodes (GF/ON) to exhibit optimal electrocatalytic properties. The VRFBs assembled with GF/ON (GF/ON-PN) achieved an EE of 64.9% at 260 mA cm^{-2}, and the obtained electrochemical performances, including discharge capacity, cycling stability, and circuit impedance, are superior to those of commercial brand-new GF electrodes. This strategy of N and O co-doping through the dual molten salt medium provides a practically valuable reference for subsequent preparations of high-performance VRFB electrodes.

Surprisingly, some halogen atoms such as Br, Cl, and F can be doped into the edge of the carbon structures, thereby promoting charge transfer and electrocatalytic reactions.[49] Park *et al.* prepared halogenated graphene nanoplatelets (F-, Cl-, and Br-GNP) by ball milling in the atmosphere of F_2, Cl_2, and Br_2, respectively.[32] The performances of these three groups of halogenated graphene nanoplatelets follow the order Br-GNP > Cl-GNP > F-GNP. The performance of the Br-GNP electrode is excellent, with a capacity retention rate of 86.8% at 50 mA cm^{-2}. This new method shows a new perspective for preparing high-performance VRFB electrodes through heteroatom doping. Heteroatom doping is an efficient modification process that can accurately introduce specific heteroatoms to optimize material properties. However, there are some disadvantages in heteroatom doping, such as low doping efficiency, many side reactions, complex processes, and high costs. Currently, many new doping techniques are expected to solve the above problems. For example, the ion implantation method can precisely control the doping position and concentration of heteroatoms. The plasma treatment can help improve the doping efficiency, and the chemical vapor deposition (CVD) can uniformly dope heteroatoms on the surface of the material. The molten salt activation system can not only uniformly dope but also construct a multi-dimensional pore structure.[50,51] Among these, the molten salt activation system treatment process is relatively simple, which can achieve the construction of pore structures and the uniform doping of heteroatoms. It is a very promising strategy among the new heteroatom doping methods in our opinion.

3.1.2 Design of pores. At present, the SSA of commercial PFFEs ranges from 0.1 to 1 $m^2 g^{-1}$, significantly lower than that of other porous carbon materials, which exceeds 1000 $m^2 g^{-1}$.[52] PFFEs with a large SSA often exhibit excellent electrochemical performance, mainly due to the abundance of active sites afforded by the high SSA, which enhances the electrode performance. Moreover, since the pore structures of PFFEs are related to the SSA of the material, and chemical reaction sites and ion transport channels on the material surface, a reasonable pore size, pore tortuosity, and porosity would affect the performance of PFFEs, which will be discussed one by one below.

3.1.2.1 Pore size. In the structure of carbon materials, according to the standards of the International Union of Pure and Applied Chemistry, the pore size can be divided into macropores (>50 nm), mesopores (2–50 nm), and micropores (<2 nm).[53] The presence of macropores will improve the permeability of the material, but will reduce the SSA of the

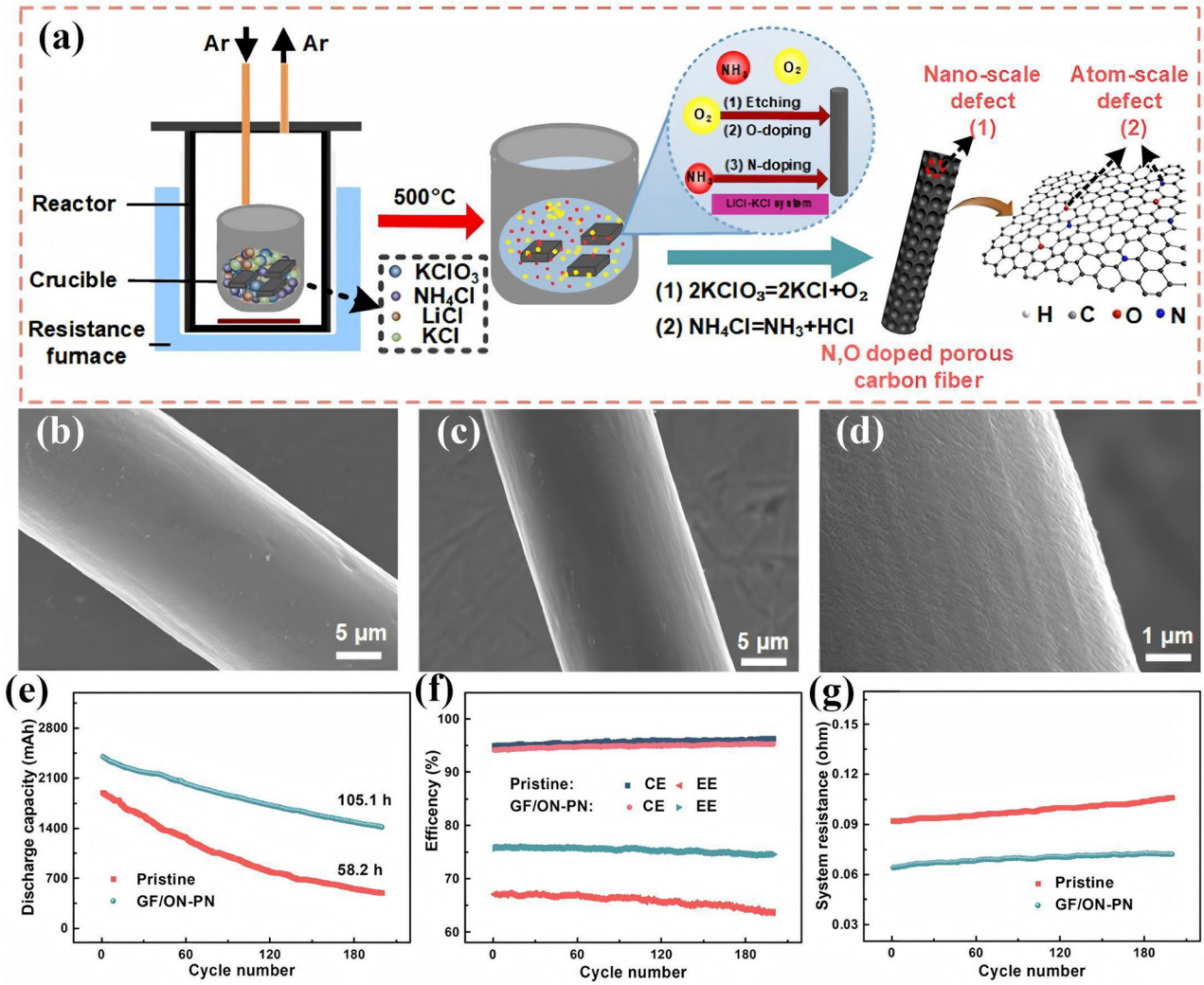

Fig. 5 (a) Schematic diagram of the process of preparing N- and O-doped CF electrodes by the molten salt system. SEM images of (b) GF and (c) and (d) GF/ON. (e) The discharge capacity of pristine and GF/ON-PN at 260 mA cm^{-2}, and (f) efficiency (CE and EE) and (g) system resistance of pristine and GF/ON-PN at 140 mA cm^{-2} for 200 cycles.[31] Copyright (2024). Wiley-VCH.

materials. The presence of micropores increases the SSA of the materials and facilitates charge transfer, but leads to poor permeability. Mesopores are the bridge between macropores and micropores.[54] There is a subtle relationship between the size of the pore, the SSA of the material, and permeability. Therefore, the trade-off between material permeability and SSA should be made when designing the pore size structures.

Specifically, in VRFBs, the migration processes of vanadium ions in the pore size are as follows. (i) Vanadium ions follow the electrolyte flow to the void regions of the reaction sites on the electrode material surface. (ii) Vanadium ions diffuse from the inside of the solution to the electrode–electrolyte interfaces. (iii) Redox reactions occur at the electrode–electrolyte interfaces. Notably, in process (iii), pore structures with a size of 50–100 nm can effectively eliminate the ion diffusion limitation caused by the space effect.[55] Meantime, redox reactions usually occur in mesopores of 5–10 nm.[56] Therefore, the pore structures of PFFEs should be multi-scale and multi-dimensional. Wu *et al.* used Zn metal compounds to construct CF electrodes with multi-dimensional pores (MPNCF-5), as shown in Fig. 6.[34] MPNCF-5 can facilitate the swift infiltration of electrolytes, enhancing the diffusion efficiency and the redox reaction rate of vanadium ions within the mesopores/nanopores. After testing, the SSA of MPNCF-5 is as high as 4.586 cm^2 g^{-1}, *i.e.*, 9 times that of ordinary CF electrodes, and the charge transfer resistance (R_{CT}) of MPNCF-5 electrodes is 68.7 mΩ cm^2. In addition, the VRFBs with MPNCF-5 electrodes can achieve an EE of 81.9% at 320 mA cm^{-2}, which is 15.2% higher than the EE of the original CF electrodes (66.7%). Even at 320 mA cm^{-2}, the MPNCF-5 electrodes can undergo 500 long-term cycles without significant attenuation of energy density.

The combination of multi-scale and multi-dimensional pore structures is an effective strategy to balance the SSA and permeability of electrodes. In terms of designing pore structures, some novel strategies may help achieve the formation of

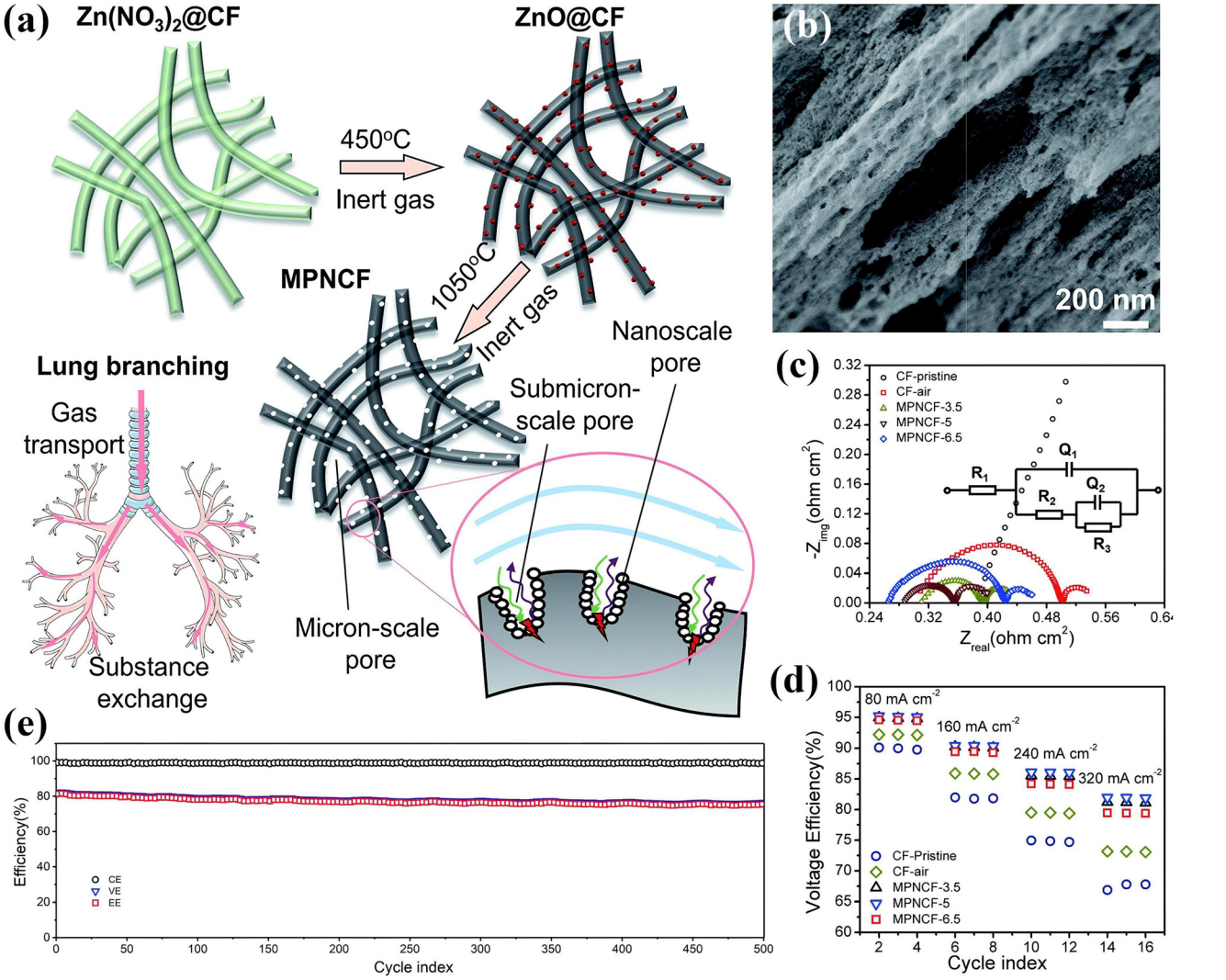

Fig. 6 (a) Diagram of the preparation of porous CF electrodes. (b) SEM image of MPNCF-5. (c) Electrochemical impedance spectra of different batteries. (d) EE. (e) EE, VE, and Coulomb efficiency (CE) of the battery after 500 cycles at 320 mA cm^{-2}.[34] Copyright (2018). Royal Society of Chemistry.

multi-level pore structures. (i) Materials with multi-dimensional complex structures are selected as precursors for the preparation of electrodes. The complex structures of the precursor are expected to endow carbon materials with multi-dimensional structures.[53] (ii) The preparation of materials is in combination with multi-dimensional pore-forming agents. For example, MgO and SiO_2 contribute to the formation of micropores in materials, while some gases such as CO_2 contribute to the formation of macropores in carbon materials.[33,55,57] Therefore, we believe that using multi-dimensional complex materials as precursors and regulating the pore structure of materials with efficient multi-dimensional pore-forming agents and activators is a very promising strategy in pore structure design and formation.

3.1.2.2 Pore tortuosity. Pore tortuosity is a usually overlooked factor in the study of PFFEs. The influence of pore tortuosity on electrode materials is mainly reflected in the SSA of the material, and the flow rate and concentration distribution of the electrolyte. Combined with the relationship between tortuosity and velocity, the corresponding tortuosity formula can be constructed:

$$\tau = \frac{\sum \sqrt{u_x^2 + u_y^2 + u_z^2}}{\sum |u_x|}$$

where τ is the tortuosity, u is the velocity, and x, y, z denote the corresponding directions.[58] Typically, large tortuosity can impede the flow of the electrolyte and affect the permeability, resulting in a large transmission resistance. Based on 3D modeling, Wang *et al.* compared the velocity distribution, concentration distribution, and current distribution in cylindrical, slit, and spherical pores.[59] The results show that the cylindrical pore structures have the maximum current density, the most uniform flow rate, and the smallest pore tortuosity at the same voltage. Although pore tortuosity is not a decisive factor in the performance of an electrode, it can still be used as

a small strategy to optimize the electrodes. Some template strategies are expected to improve the tortuosity of materials, *i.e.*, using long and straight nanorods as templates for constructing the pore structure of materials.[60] In addition, it is also necessary to pay attention to the degree of compression of the materials, and a high degree of compression will increase the bending of the material.[61]

3.1.2.3 Electrode structure porosity. The structure porosity of electrodes can also significantly affect the performance of the electrodes. High porosity reduces the SSA of the material but promotes electrolyte delivery. In addition, the structure porosity can also affect factors such as electrolyte concentration, velocity, and current density. Trade-offs in porosity designs to achieve optimal electrode performance require big data to build the model.

A study compared three different structure porosity types of electrodes: uniform porosity, low structure porosity at the inlet of the electrolyte, and low structure porosity at the outlet of the electrolyte. The outcomes show that VRFBs with electrodes showing low structure porosity at the inlet of the electrolyte have the highest EE.[62] Alphonse *et al.* numerically investigated the effect of increasing structure porosity on the potential of electrodes, overpotential, current density, and species concentration in VRFBs during the process of discharge by establishing the data models of equilibrium state. Four types of electrode structure porosity distributions were set up in the experiment: (i) the porosity of both the positive and negative electrodes is constant and the value is the same (set to 94%); (ii) the porosity of the negative electrode increases from 64% to 94% with the electrode thickness (increasing gradually by 10%), while the porosity of the positive electrode remains at 94%; (iii) the porosity of the positive electrode increases from 64% to 94% with the thickness of the electrode (increasing gradually by 10%), while the porosity of the negative electrode remains at 94%; and (iv) the porosity of both the positive and negative electrodes gradually increases from 64% to 94% with the electrode thickness (increasing gradually by 10%). It is found that the batteries in the fourth case exhibit the highest potential performance, lowest overpotential, and most uniform current distribution compared to the previous three cases. Therefore, hierarchical porous structures are indispensable for the high performance of materials.

Here, some advanced technical strategies are expected to solve the rational manufacturing of structure porosity, such as the use of AI-enabled 3D printing technology, which is expected to achieve precise control of porosity. Introducing some organic framework structures such as MOFs into materials is also an effective strategy for constructing precise porosity and pore structures.

3.2 Introduction of catalysts

The modification strategies of intrinsic treatment can improve the performance of PFFEs by increasing the number of active sites, SSA, *etc.*[63] However, due to the limited increase in the number of active sites and SSA, there are also limitations to the performance optimization of intrinsic treatment, which cannot meet the needs of high-performance electrodes. Surprisingly, the introduction of catalysts can accelerate the speed of specific reactions and improve the catalytic activity of PFFEs, thus significantly improving the overall performance of PFFEs. Currently, the types of catalysts include carbon-based catalysts, metal catalysts, metal oxide catalysts, metal carbide catalysts, and other special catalysts. These catalyst materials each have their own advantages, and can effectively tune the performance of PFFEs.

3.2.1 Carbon-based catalysts. Carbon-based materials have the characteristics of abundant sources and diverse morphologies, and are often used as catalysts to modify PFFEs. Carbon-based catalysts catalyze redox reactions by adhering to the PFFEs, thereby enhancing the comprehensive performance of VRFBs.[64] Here, in this review, carbon-based catalysts are divided into zero dimension (0D), one dimension (1D), two dimension (2D), and 3D according to the dimensions of the catalysts in the following discussions.

3.2.1.1 0D carbon-based catalysts. 0D carbon-based materials such as carbon quantum dots and fullerenes are the new generation of carbon-based materials. Their surface/interfacial effects, scale effects, and macroscopic quantum tunneling effects make them exhibit superior optoelectronic and mechanical properties, compared to conventional materials, and are widely used in electronics, catalysis, and other fields.[65] Fullerene is a hollow molecule composed of carbon, whose nanosize and specific morphology endow it with a large SSA, high conductivity, good thermal conductivity, and special mechanical properties. In addition, the surface of fullerene has a rich electron cloud, which can interact with ions, thereby promoting the adsorption of ions.[66,67] Meantime, the electron cloud can also coordinate with ions to form stable complexes, further enhancing the adsorption of ions. Diwany *et al.* first proposed the application of fullerene as a catalyst in VRFB electrodes and achieved efficient catalysis of VO^{2+}/VO_2^+.[68] Characterization test results showed that each fullerene has a spherical structure with a size of less than 1 nm. Notably, fullerene is mainly sp^2 hybridized graphite carbon with some oxygen-containing functional groups, which make the material have abundant active sites and high conductivity. The high conductivity and special electron cloud structure of fullerene greatly improve the adsorption and catalytic performance of the material for vanadium ions. Furthermore, researchers found that, in a mixed acid electrolyte, the fullerene-modified materials have high stability and can prevent the precipitation of toxic chlorine in side reactions. This work opens up the way for the development and application of fullerene catalysts in VRFB electrode materials.

Similarly, as an important part of 0D carbon-based materials, carbon quantum dots have attracted the attention of researchers due to their ultra-small size, large SSA, and rich surface (edge) defects. Zhou *et al.* first reported the preparation of carbon dot-modified GF (CD/GF) electrodes by a one-pot solvothermal method.[69] The doping mechanism of the one-pot

solvothermal method is that during the solvothermal reaction process, carbon source molecules undergo reactions such as polymerization and carbonization in a high-temperature and high-pressure environment, thus forming carbon dots distributed on the GF surface. With a size of approximately 3–6 nm, these carbon dots are evenly distributed on the surface of GF, transforming it from a surface-ordered to a surface-disordered CD/GF structure. Moreover, the modification of CDs introduces a large number of defects into the electrode surface, significantly enhancing the hydrophilicity of CD/GF and increasing the adsorption of vanadium ions on the electrode. The high conductivity and stability of CDs also promote CD/GF to exhibit low R_{CT} and high stability. Through electrochemical tests, the battery assembled with the CD/GF electrode was found to have an EE of 52.2% at a current density of 350 mA cm^{-2}, and after 1000 long cycles at 150 mA cm^{-2}, the EE still remained at 74%. In addition, this battery can adapt to work in a variety of temperature environments and has great application potential.

Although 0D carbon-based catalysts have been widely used in photocatalysis, biopharmaceutical catalysis, and other fields, there are still few studies on the modification of PFFEs in VRFBs. In the above studies, both fullerene and carbon quantum dots have a positive effect on the conductivity and stability of electrode materials, and also make a significant contribution to the catalytic performance. Therefore, it is necessary to study the application of 0D carbon-based catalysts in the modification of PFFEs. Further studies can focus on these materials and deeply analyze the contribution of size effects to the modification effect, which will be valuable work.

3.2.1.2 1D carbon-based catalysts. The traditional carbon-based electrodes have poor electrocatalytic activity, small SSA, and poor hydrophilicity. Therefore, at high current densities, they cannot meet the need for rapid transmission of a large number of charges and efficient catalysis. Notably, the unique tubular structures of 1D carbon-based materials shorten the transmission path of charges and improve the ion diffusion rate. Moreover, these materials also have a large SSA and excellent stability, which make them favored by researchers. 1D carbon-based materials can be divided into three categories according to diameter: carbon nanotubes (CNTs) with a diameter less than 50 nm, carbon nanofibers (CNFs) with a diameter between 50 and 200 nm, and carbon fibers with a diameter greater than 200 nm.[70]

CNTs possess a large number of sp^2-hybridized and graphite-like hexagonal carbon ring network structures, which have a positive effect on the transmission of charges and the adsorption of ions. Zhang *et al.* using ZIF-67 arrays as precursors and melamine as the nitrogen and carbon source, and under the regulation of Co^{2+} ions, uniformly constructed N-doped CNTs (NCNT@CF) on CF through a bottom-up simple method (Fig. 7a and b).[71] Specifically, ZIF-67 arrays are first *in situ* grown on the CF substrate through a hydrothermal reaction, with Co^{2+} attached thereon. Then, melamine is pyrolyzed into carbon and nitrogen substances at high temperature, attached to ZIF-67, and eventually evolved into N-doped CNTs. During this process, Co^{2+} is converted into the catalyst Co, which promotes the generation of CNTs. This doping method enables CNTs to be fully and uniformly attached to the electrode. Adjusting the microstructure of ZIF-67 and the amount of melamine can effectively regulate the micromorphology, N doping amount, and bonding strength of CNTs. Benefiting from the superiority of NCNTs, the assembled battery exhibits an astonishing EE of up to 76.6% at 300 mA cm^{-2} and maintains long-term stability over 550 charge/discharge cycles. Introducing functional groups into CNT catalysts is an effective and commonly used means to improve the activity of CNT catalysts. Dai *et al.* modified CNTs by high-temperature activation with KOH and applied them as cathode catalysts in VRFBs.[72] Notably, the doping of CNTs mainly relies on the ultrasonic dispersion and impregnation drying method. Firstly, CNTs are ultrasonically dispersed in the solvent. Then, the GF is immersed in the solvent and dried to obtain CNT doped GF. Moreover, the activation of KOH introduces oxygen-containing functional groups and a large number of defects in CNTs. These oxygen-containing functional groups provide active centers for the electrode and optimize the hydrophilicity of the material, thereby enhancing the adsorption and catalysis of vanadium ions. Notably, some other functional groups, such as borate-based, phosphate-based, and sulfonic acid-based functional groups, also promote the adsorption and catalysis of vanadium ions by providing reaction sites for the electrode and enhancing the hydrophilicity of the electrode.[73–76]

Unfortunately, in the application field of CNT catalysts, problems such as weak adhesion and morphology fragmentation are often encountered, which limit the application of CNT catalysts. Therefore, solving the problems of firmly and efficiently adhering CNTs to the PFFEs is an urgent task. Organic binders can fix CNTs on the CF relatively well, but the introduction of binders will hinder the transport of ions and affect the catalytic performance.[78] To avoid the influence of foreign impurities on catalytic performance, researchers innovatively used *in situ* formed sucrose pyrolysis carbon as a binder to fix CNTs and GF.[79] The composition of this binder mainly consists of carbon materials similar to CNTs and GF, therefore featuring high adhesiveness and low contact resistance. Recently, a new *in situ* growth strategy has also been used to introduce CNT catalysts, and this method can uniformly fix CNT catalysts without the need for binders. Liu *et al.* uniformly introduced N, B-doped CNTs (NBCNTs) on the surface of CF by using an *in situ* growth strategy, as shown in Fig. 7c–e.[77] The mechanism of *in situ* growth of CNTs is to immerse CF in a growth solution prepared from urea, polyethylene glycol and boric acid, and then carbonize CF at high temperature. At high temperature, the growth solution will first generate B, N co-doped carbon nanosheets. During annealing, thermal stress appears in the carbon nanosheets due to the difference in the cooling rates of different parts. When the thermal stress is greater than the yield limit of the carbon nanosheets, they will curl to form NBCNTs. By adjusting the ratio of N and B, the morphology of CNTs can be designed, and they can be fixed on the surface of CF by *in situ* growth, avoiding the influence of binders. The EE

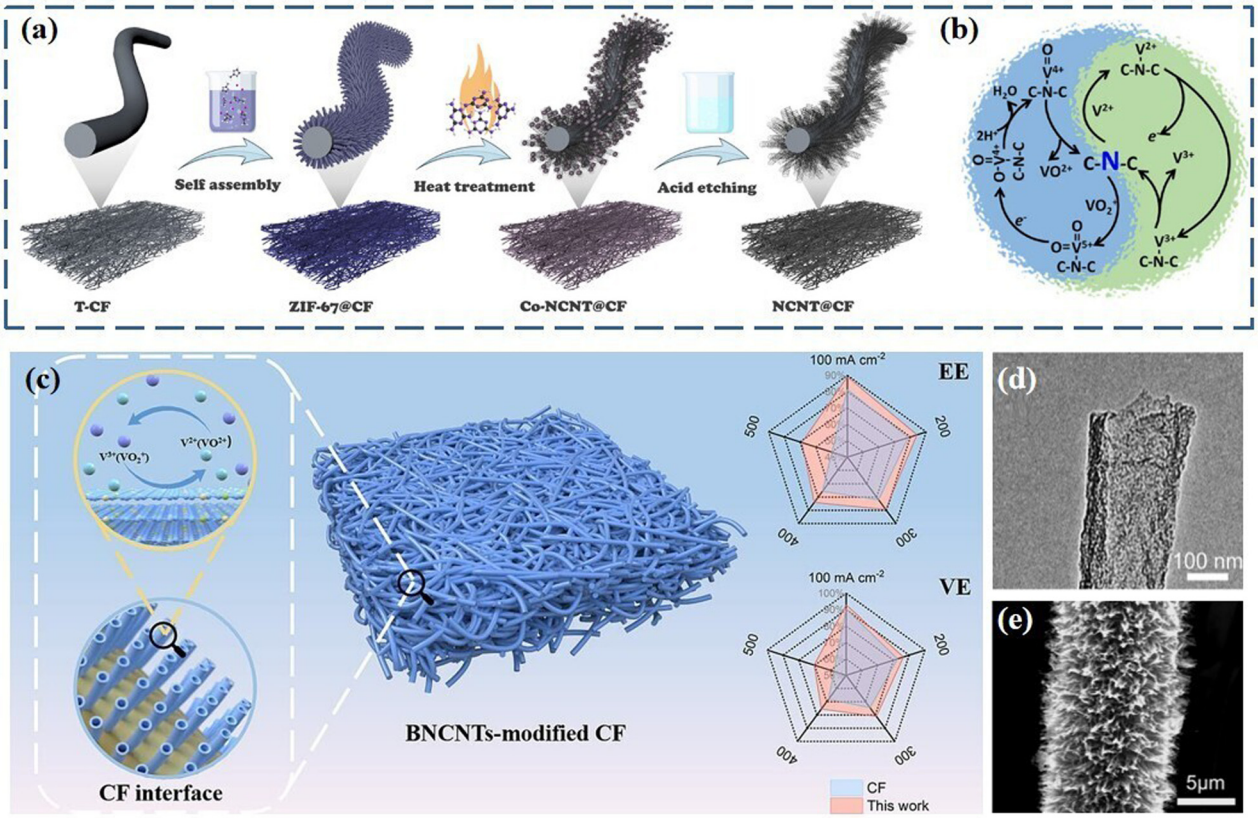

Fig. 7 (a) Flow chart of the preparation process of NCNT@CF. (b) Catalytic mechanism of N-doping on vanadium ions.[71] Copyright (2024). ACS Publications. (c) Flowchart of NBCNTs' topography design and corresponding EE and VE performance; (d) TEM and (e) SEM image of NBCNTs.[77] Copyright (2023). Elsevier.

of the VRFBs assembled with NBCNTs is 79.3% at 300 mA cm^{-2}, and even remains at 68.7% at 500 mA cm^{-2}. In addition, after 1000 long cycles of testing at 300 mA cm^{-2}, the EE shows almost no attenuation.

Compared to CNTs, CNFs have larger sizes and are commonly used to prepare PFFEs, while less used as catalysts to modify PFFEs.[80,81] However, some studies still explored the improvement effect of CNFs on the performance of VRFBs after compositing with PFFEs. Zhang *et al.* reported a strategy of wrapping carbon nanofiber networks around CF electrodes using the self-assembly process of polyaniline.[82] This method does not require a binder and introduces N, S-doped porous carbon nanofiber networks to CF electrodes. Owing to the abundant active sites introduced by heteroatoms and the interconnected channels provided by the CNF network, the prepared electrodes exhibit an EE of 82.4% at a current density of 320 mA cm^{-2}. Moreover, the electrodes also show excellent long-term stability over 1000 cycles. In addition to constructing the CNF network, Xu *et al.* proposed to construct a dual-gradient CNF/GF composite electrode structure to optimize the performance of VRFBs.[83] The construction of the dual-gradient CNF/GF composite electrode involves introducing more CNFs on the side of the GF electrodes close to the membrane and less CNFs on the side close to the plate. The former relies on the high catalytic activity of CNFs to promote the redox reactions of vanadium ions in VRFBs, and the latter utilizes the high conductivity of CNFs to promote charge conduction. In addition to the macro-gradient distribution of CNFs on the GF, this work also radially micro-gradiently distributed CNFs along individual fibers. This macroscopic and microscopic gradient distribution strategy greatly reduces the resistance and improves the performance of VRFBs. After testing, these electrodes were found to show the lowest ohmic resistance, contact resistance, and R_{CT}. The assembled battery exhibits an EE of 81.84% at a current density of 300 mA cm^{-2} and has a peak power density of 1109.5 mW cm^{-2}. Notably, the modified electrodes also show far superior cycle stability and rate performance compared to commercial PFFEs.

The morphology and performance of 1D carbon-based catalysts play an important role in improving the performance of PFFEs. Currently, there are still shortcomings in the introduction of 1D carbon-based catalysts, such as the inability to firmly adhere the catalyst to the PFFE surface, the morphology of the catalyst hindering the flow of electrolytes, and complex preparation processes. Subsequent works can explore these directions in-depth, such as precisely regulating the morphology of 1D carbon-based catalysts with the help of the *in situ* characterization instruments and advanced preparation processes, introducing functional groups and defects into 1D carbon-based

catalysts, and constructing high-performance 1D carbon-based catalyst/PFFE composite electrodes.

3.2.1.3 2D carbon-based catalysts. 2D carbon-based materials (graphene, graphite sheets, *etc.*) have received favor from researchers in recent years and are widely used in the fields of energy, catalysis, biology, *etc.* In the PFFE modification strategy, 2D carbon-based catalysts are highly desirable, which is closely related to their special structures, and excellent physical and chemical properties. The surface of 2D carbon-based materials has abundant covalent bonds, which facilitate electron transfer, making the PFFEs have high conductivity. Secondly, the large 2D plane provides a lot of space for the attachment of active sites and chemical reactions that optimize the overall catalytic performance of the PFFEs.[84] Moreover, the strong acid–base inertness of these catalysts enables them to adapt to many electrolytes and expands their application range.

Graphene is a type of 2D carbon nanomaterial, which exists as single layer and multilayer graphene as well as graphene oxide (GO), reduced graphene oxide (rGO), *etc.*[85] Graphene is composed of hexagonal honeycomb lattices of carbon atoms with sp^2 hybrid orbitals, featuring a large SSA, high conductivity, and rich edge defects. Xia *et al.* deposited commercial graphene catalysts on the surface of CF electrodes through the solution coating method, and used them as the positive electrode (G/CF) of VRFBs to catalyze the VO^{2+}/VO_2^+ redox reactions.[86] The G/CF electrodes significantly enhance the catalytic performance of the VO^{2+}/VO_2^+ redox reactions and reduce the ohmic polarization during the charge–discharge processes. The prepared VRFBs exhibit a peak power density of approximately 325 mW cm^{-2}, which is 39 mW cm^{-2} higher than that of pure CF. Additionally, the VRFBs maintain the EE above 80% after 500 cycles at a current density of 80 mA cm^{-2}. Notably, optimizing the graphene catalysts before introducing them to CF can significantly improve the modification effect. Fu *et al.* coated CF electrodes with Ar plasma-treated multi-layer graphene (Ar-GCF) *via* CVD, as shown in Fig. 8a–c.[87] Specifically, methane was cracked in a mixture of methane and hydrogen at 1040 °C, depositing carbon atoms on CF to form carbon felt loaded with multilayer graphene (GCF). Then, GCF was treated with argon plasma to obtain the modified electrode material Ar-GCF. Ar-GCF has numerous defects and oxygen-containing functional groups, causing electrons on the material surface to tend to distribute near the O-containing functional groups, greatly enhancing the conductivity of the electrode materials. The power density, EE, and voltage efficiency (VE) of the VRFBs assembled with Ar-GCF are 1130.09 mW cm^{-2}, 87.16%, and 89.11%, respectively, outperforming the commercial pristine CF electrodes. More importantly, the R_{CT} of the Ar-GCF electrodes increases by only 15.79% after 800 cycles, while the R_{CT} of the commercial pristine CF electrodes increases by 102.40% after 600 cycles, which strongly demonstrates the excellent stability of the Ar-GCF electrode in VRFBs. Some heteroatoms have also been used to modify the graphene catalysts. Li *et al.* introduced N-doped rGO (N-rGO) into GF electrodes (N-rGO/GF) by the freeze-drying method using urea as the nitrogen source.[88] Notably, the rGO in this work was prepared as follows. First, GO was made by the Hummers' method using graphite powder, sodium nitrate and concentrated sulfuric acid, and a GO solution was obtained after the reactions. Then, the GF electrode was soaked in the urea–GO solution, followed by freeze-drying and pyrolysis in a nitrogen atmosphere tube furnace for the conversion of GO to rGO and nitrogen doping, getting the N-rGO/GF electrode. Owing to the synergistic effect of nitrogen atoms and graphene catalysts, N-rGO/GF exhibits a large SSA and a high density of active sites, significantly enhancing its catalytic performance for the $VO^{2+}VO_2^+$ reactions.

Although the modification effect of graphene catalysts on PFFEs is excellent, complex processes and high costs limit their development. To realize industrialized and large-scale production as soon as possible, many researchers have made great contributions. Long *et al.* proposed a method for large-scale preparation of G/CF electrodes by the CVD method, and reached a scale of 20 cm × 20 cm, as shown in Fig. 8d–f.[89] The specific CVD method is as follows. H_2 and CH_4 are introduced into the tube furnace where CF is placed at a ratio of 20 : 3 under high temperature. CH_4 decomposes into carbon atoms in the high temperature and H_2 atmosphere and grows on the surface of CF to form graphene. Surprisingly, the EE of this electrode at a current density of 100 mA cm^{-2} is 86.37%, and the peak power density reaches 1189 mW cm^{-2}. These achievements are encouraging. Unfortunately, in the field of graphene catalyst applications, the π–π bond stacking interaction and strong van der Waals force between the graphene layers cause these materials to easily suffer from problems such as agglomeration, thereby reducing the SSA and affecting performance.[90] Advanced 3D fabrication techniques, such as the formation of vertical graphene on PFFE surfaces and the incorporation of porous graphene, are expected to address the issue of graphene agglomeration. These optimized 3D strategies are described in the next section.

3.2.1.4 3D carbon-based catalysts. 3D carbon materials are widely used in the fields of electrochemistry and electrocatalysis due to their high SSA and rich pore structures. Therefore, 3D carbon-based catalysts are also commonly used to modify PFFEs. These porous structures endow 3D carbon-based catalysts with large reaction contact area and fast ion transfer channels, which can effectively improve the catalytic efficiency. This section mainly elaborates and analyzes some highly concerned 3D carbon materials, such as 3D graphene catalysts, C–C composite catalysts composed of multi-dimensional carbon materials, and green and efficient bio-carbon-based catalysts.

(i) 3D graphene catalysts. The porous structures of the 3D carbon-based catalysts can not only effectively promote ion transfer but also improve the aggregation problem existing in the 2D graphene catalyst. Porous graphene is also called the graphene nanonetwork, which is characterized by a rich multi-dimensional pore structure inside. Compared with traditional graphene, porous graphene has a larger SSA, more active sites, and more edge defect structures.[91] The performance

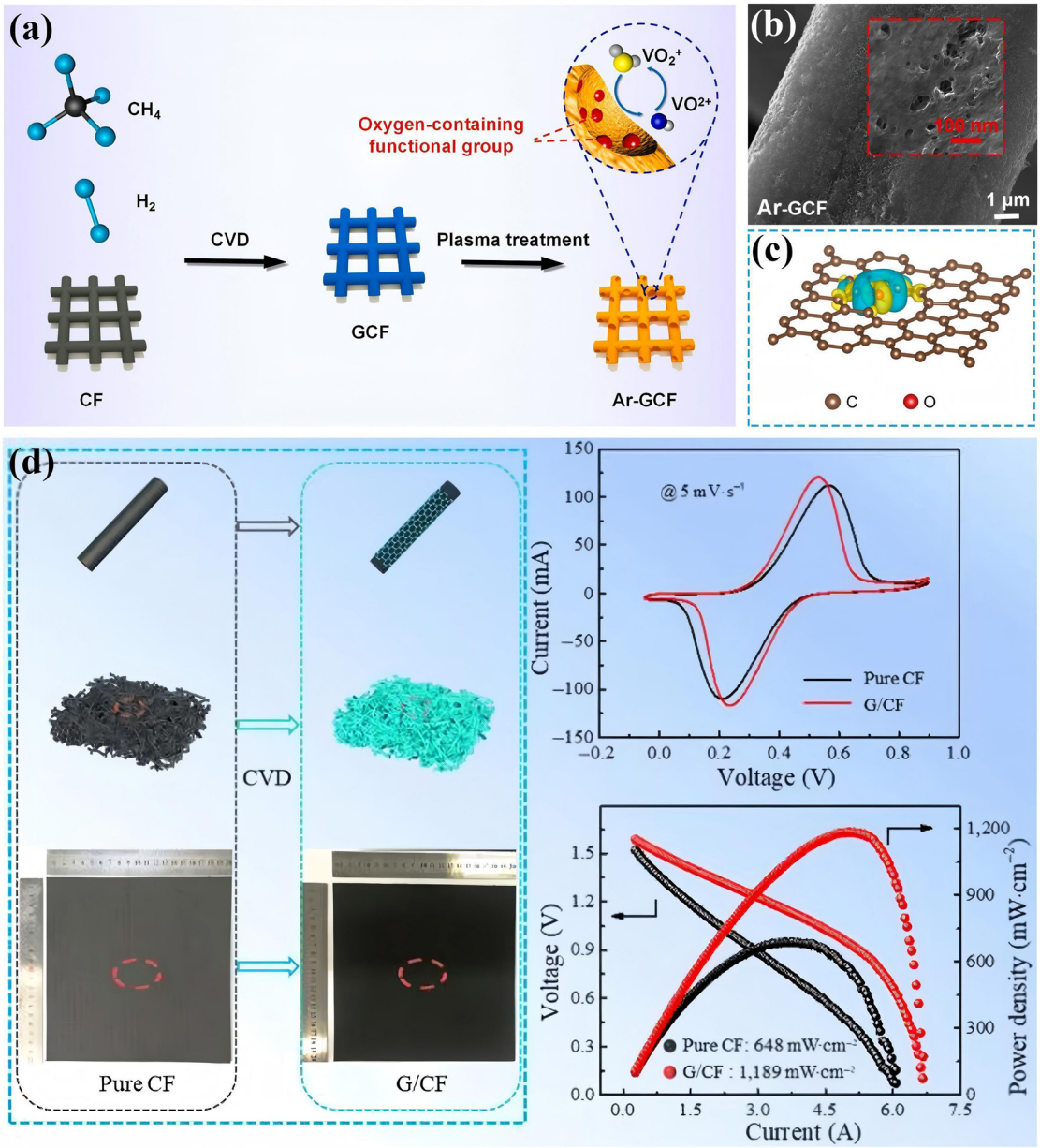

Fig. 8 (a) Flowchart of Ar-GCF preparation. (b) SEM image of Ar-GCF. (c) O–graphene charge density difference (the yellow area indicates increased electron density, the cyan area indicates decreased electron density).[87] Copyright (2023). Elsevier. (d) Schematic diagram of graphene modification. (e) CV of pure CF and G/CF. (f) Peak power density of pure CF and G/CF.[89] Copyright (2021). Springer Nature.

improvement brought about by the porous structure of porous graphene can well counteract the negative effects brought about by graphene agglomeration and empower itself. Opar *et al.* introduced N-doped graphene onto CF electrodes (NMG-CF-7) through a simple hydrothermal process, and constructed an N-doped 3D porous graphene CF electrode (NMG-CF-7) under high-temperature pyrolysis, which was applied to VRFBs.[92] Owing to the special structures of porous graphene, NMG-CF-7 exhibits a large SSA (19.45 $m^2\ g^{-1}$) and a rich pore structure. The porous structures with a large SSA can increase the number of active sites and reduce the mass transfer resistance of vanadium ions and ohmic polarization, enabling the electrode to show improved electrochemical performances even at high current densities. Electrochemical tests show that NMG-CF-7 has an EE of 75.1% at 150 mA cm^{-2}, with excellent rate performance and cycling stability. The emergence of porous graphene points out the direction for the high-performance commercial application of graphene.

In addition, the rational distribution of graphene catalysts can also offset the negative effects of graphene agglomeration. Guo *et al.* proposed a metal-free catalytic CVD strategy for *in situ* growth of vertical porous N-doped graphene on GF.[93] The specific growth mechanism is as follows. Using CH_4 as the carbon source and H_2 as the reducing gas, 2D graphene will

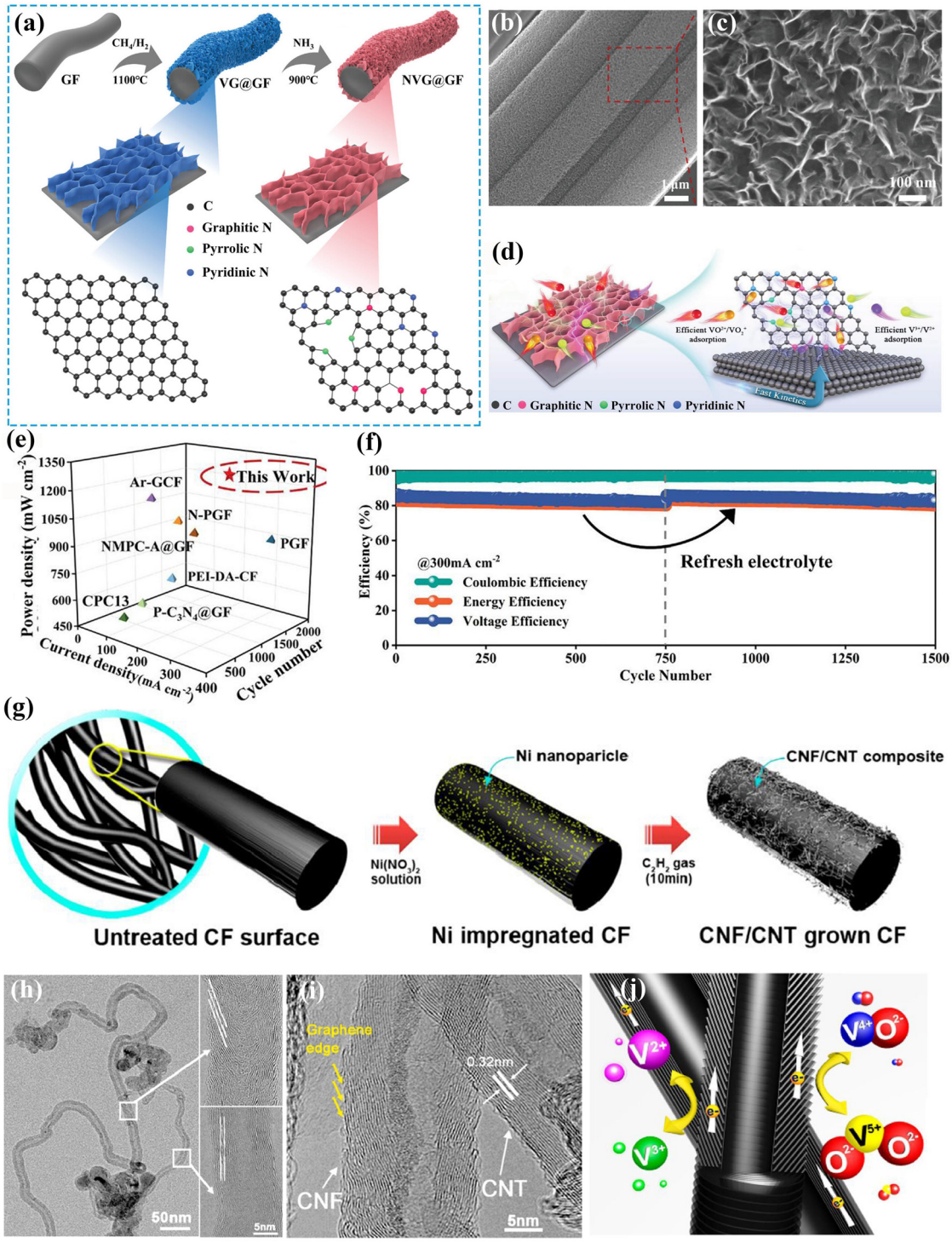

Fig. 9 (a) Schematic illustration of the preparation process, (b) and (c) SEM images, (d) structural advantages, (e) cycle stability and peak power density comparison with advanced nano carbon-modified electrodes, and (f) cycle performance at 300 mA cm^{-2} of the NVG@GF electrode.[93] Copyright (2024). Wiley-VCH. (g) Flowchart of the synthesis of CNFs/CNTs grown on the surface of CF decomposed by C_2H_2 gas with the assistance of Ni nanoparticles. (h) HRTEM image of a CNF/CNT composite, with the inset showing the CNF and CNT sidewalls (white line: graphene layer orientation). (i) The coexisting structures in the CNF/CNT, respectively. (j) Schematic diagram of the advantages of CNF and CNT composite structures in catalyzing vanadium ions.[94] Copyright (2013). ACS Publications.

grow *in situ* on GF at a high temperature of 1100 °C. After the temperature drops to 900 °C, NH_3 is introduced into the tube furnace. This will etch the grown graphene and introduce nitrogen atoms, forming N-doped 3D porous graphene. As shown in Fig. 9a–f, the introduced porous graphene catalysts are vertically, evenly, and tightly distributed on the GF

materials. The reasonable distribution not only effectively improves the graphene agglomeration problem but also avoids the uneven coverage of active substances. In addition, the vertical multi-dimensional structures also provide channels for the large and rapid transport of charges, improving conductivity. Electrochemical tests show that the EE of the electrode material (NVG@GF) is 87.1 and 83.3% at 200 and 300 mA cm^{-2}, respectively, with a peak power density of 1308.56 mW cm^{-2}, which is superior to the modified electrode of carbon nanomaterials in the existing reports of VRFBs. More importantly, the decrease in EE caused by long-term cycling can be restored to the initial value by renewing the electrolyte. The many advantages of NVG@GF electrodes reveal their great value in the commercial field.

Notably, some high-performance graphene-modified PFFEs, such as porous graphene-modified PFFEs and vertical graphene-modified PFFEs, still have problems such as the complex preparation process. It is urgent to improve the current preparation methods such as template-assisted methods, self-assembly methods, and CVD methods, and apply them to actual production.[95]

(ii) C–C composite catalysts. C–C composite-based catalysts refer to composite catalysts composed of different types of 3D carbon-based materials. Different types of carbon-based materials have different advantages, and the combined carbon-based materials can play a synergistic role, making the C–C composite-based catalysts exhibit high performance.

Although CNFs and CNTs are both 1D carbon-based materials, they have different electrochemical characteristics. Due to the inclination of the graphene layer relative to the fiber axis of CNFs, CNFs expose edge planes with a large number of defects, which provide abundant active sites for ion adsorption and reaction on the outer surface of CNFs. Similarly, the graphene sheets of CNTs are composed of relatively inert basal planes, which endow CNTs with high conductivity and stability.[96] The composite catalysts of CNFs and CNTs can give full play to the synergy and jointly improve the catalytic performance of VRFBs. Park *et al.* introduced a CNF/CNT composite catalyst on the surface of CF by acetylene gas pyrolysis and applied it as an electrode in VRFBs, as shown in Fig. 9g.[94] The specific method for loading CNFs/CNTs on the CF substrate is as follows. The CF is nickelized to load reduced nickel and then calcined at high temperature in an atmosphere of C_2H_2 gas (carbon source). At 500 °C, the nucleation rate of acetylene is slow, and carbon atoms reach the entire nickel catalyst interface through diffusion and form CNFs without a hollow core. As the temperature rises to 700 °C, nucleation begins at the nickel metal/acetylene gas interface, resulting in the formation of CNTs, and thus the CNF/CNT composite catalyst is formed on the CF surface. The synergy between CNFs and CNTs lies in the efficient fit between the CNF outer wall with a large number of surface defects and the CNT surface for rapid electron transfer, which plays an important role in the vanadium redox reactions and significantly improves battery performance, as shown in Fig. 9h–j. Through electrochemical testing, the prepared electrodes show excellent rate performance and capacity retention at 100 mA cm^{-2}, and the battery capacity can be restored at 40 mA cm^{-2}.

Graphene is an efficient carbon-based catalyst, but it is limited by the problem of agglomeration. Other carbon-based materials combined with graphene to form C–C catalysts not only have the potential to overcome the agglomeration limitation of graphene, but also bring excellent performance improvement effects to VRFBs. Faraji *et al.* introduced functionalized CNTs (fCNTs) and GO on carbon materials by an electrochemical deposition method, and explored their catalytic activity in VO^{2+}/VO_2^+ redox reactions.[97] Specifically, the loading of GO-fCNTs is mainly achieved by using a solution rich in GO and fCNTs as the electrolyte and depositing GO and fCNTs on the graphite sheet through the galvanostatic method in a two-electrode system (the graphite sheet electrode is the working electrode and the platinum foil is the counter electrode). The introduction of GO can significantly improve the wettability of the electrode, mainly due to the large number of oxygen-containing functional groups on its surface. The introduction of fCNTs can construct a network structure on the electrode surface, which not only enhances the conductivity of the material, but also increases the SSA of the materials. In addition, the combination of fCNTs in GO also effectively improves the negative effects caused by agglomeration. Han *et al.* prepared GO and multi-walled CNT (MWCNT) composites by the electrostatic spraying method and used them to catalyze the VO^{2+}/VO_2^+ redox reactions of VRFBs.[98] The large SSA of GO combined with the complex conductive network of MWCNTs endow the modified electrode with excellent redox reversibility, ultra-low R_{CT}, and high stability.

The C–C composite catalyst can give full play to the advantages of each component of the carbon-based catalysts, and maximize the performance of the catalysts under the enhancement of the synergistic effect, which provide certain guidance for the high-performance development of the carbon-based catalyst. However, C–C composite catalysts still have disadvantages such as difficult preparation, poor mechanical properties of the material, and weak bonding of each component material. Some new processes such as the self-template method and the use of metal–organic frameworks to construct morphologies are expected to improve the dilemma of such materials.

(iii) Bio-carbon-based catalysts. Introducing heteroatoms into carbon-based catalysts can effectively improve the catalytic performance, and their intrinsic special structures can also increase the rate of charge transfer, which prompt researchers to pay attention to biomass carbon materials with rich substances and contents, and special intrinsic structures.[53] The rich substance contents of biomass enable it to have a large number of functional groups and defects without additional doping substances, which effectively simplifies the process. In addition, the special morphologies of biomass make it a natural template, which helps in the subsequent formation of multi-dimensional and multistage structures of the materials.[99]

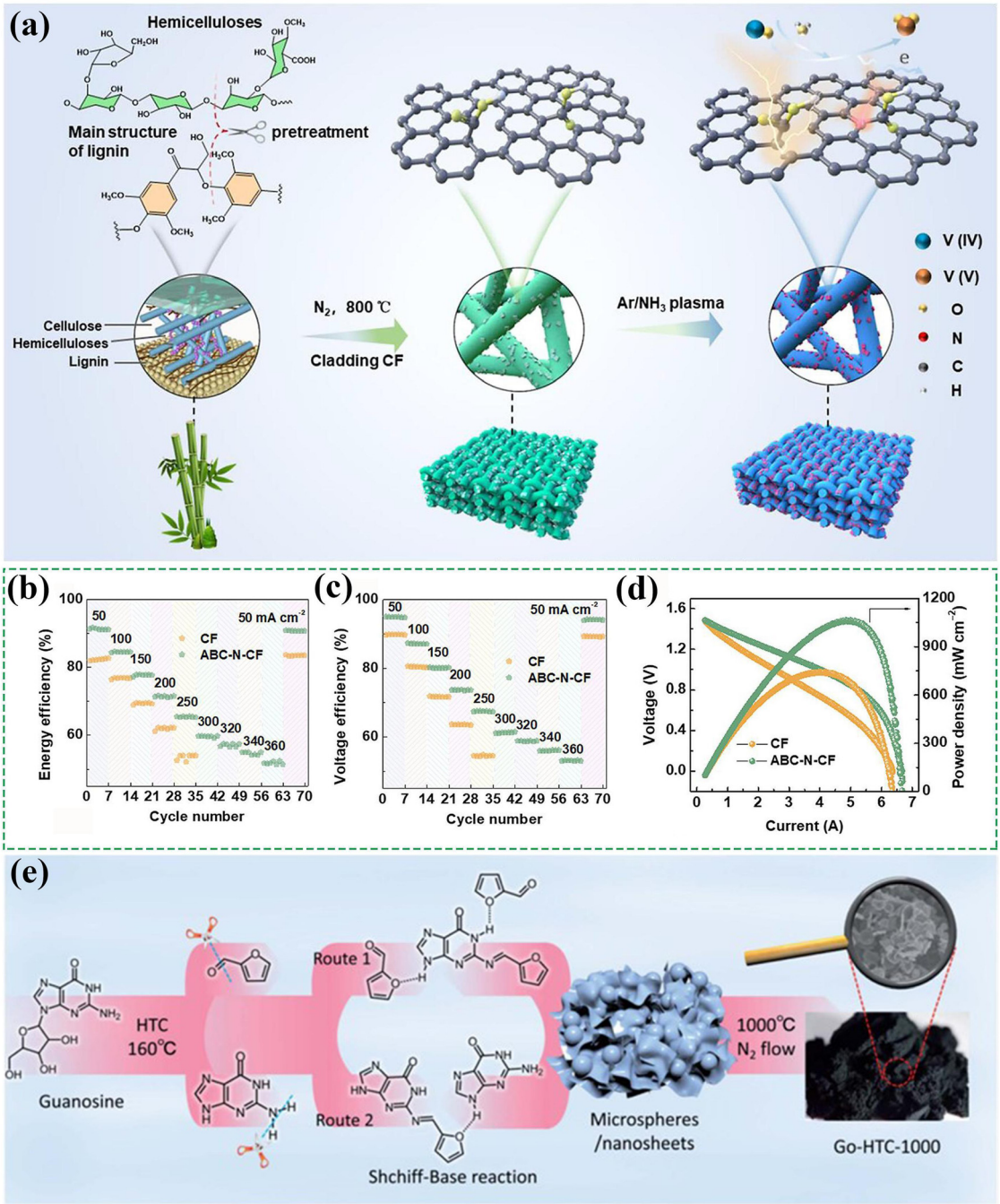

Fig. 10 (a) Process flow diagram of ABC-N-CF electrode preparation. (b) EE and (c) VE of rate performance. (d) polarization curves and power density.[100] Copyright (2024). ACS Publications. (e) Flow chart for the preparation of a unique carbon microsphere/nanosheet composite.[102] Copyright (2020). Royal Society of Chemistry.

Chen *et al.* used bamboo as a precursor to prepare an O, N co-doped hierarchical porous bamboo-based carbon modified CF (ABC-N-CF) through an acid treatment assisted plasma treatment approach, as shown in Fig. 10a–d.[100] Acid treatment can selectively remove hemicellulose and lignin in bamboo to avoid the influence of impurities on material properties. O, N co-doping provides abundant functional groups and active centers for CF materials, while the 3D porous structures introduce defects and improve hydrophilicity for CF materials, which greatly improve the catalysis, adsorption, and other properties of CF electrode materials. Benefiting from the special structures of the material, the assembled battery shows a maximum power density of 1064.6 mW cm^{-2}, which is better than the performance of the blank battery (741.9 mW cm^{-2}). Meantime, compared with the blank battery, the assembled battery shows a higher EE and VE at each current density;

especially at 250 mA cm^{-2}, the EE is 20.9% higher than that of the blank battery, showing an excellent electrochemical performance. Hu *et al.* used lotus seed shells as raw materials to synthesize hard carbon materials by pyrolysis, and densely covered them on carbon fibers to prepare modified CF electrodes (Bio-CF).[101] These electrodes have obvious catalytic effects on both V^{2+}/V^{3+} and VO^{2+}/VO_2^+ redox reactions. In addition, the Bio-CF electrodes can optimize the ion mass transfer and comprehensively optimize the performance of VRFBs. The assembled batteries provide a high EE (83.14%) and an excellent cycle stability at a current density of 100 mA cm^{-2}.

In the previous section, this review outlines the existing difficulties of C–C composite-based catalysts, such as process difficulties and high costs. To improve these problems, a simple, green, and novel process for preparing C–C composites using the intrinsic structures of biomass as templates is proposed. Huang *et al.* used bio guanosine as a precursor to prepare N-doped carbon microspheres/nanosheets by a simple hydrothermal carbonization method and loaded them on GF to improve the electrocatalytic performance of VRFBs, as shown in Fig. 10e.[102] The formation of the multi-dimensional morphologies of the carbon-based catalysts is the result of the synergistic effect of the intrinsic structures and molecules of bio guanosine under hydrothermal conditions. Among them, the construction of carbon microspheres is due to the cross-linking of a large amount of furfural and a small amount of the guanine component derived from the ribose of bio guanosine. Conversely, when the guanine component coexists with a small amount of furfural, the amino group of the guanine component undergoes a Schiff base reaction with the carbonyl group of furfural, thereby forming carbon nanosheets. Notably, this kind of carbon nanosheet shows a large SSA and a sponge-like morphology, which are closely related to the self-template effect of bio guanosine. Owing to the large SSA of the 2D carbon nanosheets and the abundant active sites provided by the carbon microspheres, the prepared electrode can still provide 66% EE at 500 mA cm^{-2}, showing a strong rate performance. In addition, in the long-term cycling test, the prepared battery has almost no attenuation in EE after 100 cycles at 100 mA cm^{-2}. This work opens up a new perspective for the application of biomass precursors in preparing C–C composites.

Bio-carbon-based catalysts have the characteristics of rich heteroatoms and special structures, which are good precursors for preparing carbon-based catalysts. However, biomass materials also have problems such as high impurity content, difficult regulation of the type and morphology of functional groups, and uneven material composition. Reasonable selection of biomass precursors, and understanding and analyzing the structures and characteristics of biomass will facilitate the application of such materials. Moreover, we summarize and compare the specific performance of the above carbon-based materials in Table 2, which has a certain reference value for the subsequent applications of carbon-based material catalysts. More importantly, we believe that depositing 3D porous graphene catalysts on PFFEs by the CVD method is a very promising modification strategy in the introduction of carbon-based catalysts.

3.2.2 Metal-based catalysts. Compared to carbon-based catalysts, although metal-based catalysts have limitations such as side reactions like hydrogen evolution, their high catalytic efficiency, high selectivity, superhydrophilicity, corrosion resistance, and recyclability still stimulate a research boom among scientists.[103,104] Currently, metal catalysts mainly consist of metal nanoparticles, such as bismuth (Bi), antimony (Sb), tin (Sn), iridium (Ir), and platinum (Pt). These nano-metal particles play an important role in enhancing the electrochemical catalytic performance of PFFEs.[103] However, the high cost and easy occurrence of hydrogen evolution reactions of some metals greatly limit their commercial applications.[105] Among these nano-metal particles, metallic Bi is widely used to modify the catalytic performance of PFFEs due to its low cost, high electrical conductivity, and good stability in acidic solutions.

Metal Bi has been proved to improve the catalysis of negative V^{3+}/V^{2+} redox reactions for VRFBs.[106] The catalytic mechanism of Bi is considered to be that Bi can generate BiH_x intermediates in the vanadium salt environment, which can catalyze the V^{3+}/V^{2+} redox reactions and inhibit the irreversible side reactions related to hydrogen, thereby improving the stability.[107,108] Although metal Bi has good stability compared with other metals, hydrogen evolution and other side reactions are inevitable in the catalytic process. Using the deposition method to embed Bi deeply into the structural network of PFFEs not only avoids the dispersion of Bi by a liquid electrolyte, but also increases the overpotential of the hydrogen evolution reaction of the battery, thereby inhibiting hydrogen evolution and improving the efficiency of the battery.[109] Li *et al.* introduced nano-Bi to the surface of GF electrodes by electrodeposition under the immersion of Bi^{3+} electrolyte ions.[110] Nano-Bi can significantly improve the performance of VRFBs by suppressing the hydrogen evolution reaction and reducing the activation energy barrier of V^{2+}/V^{3+}. Through electrochemical tests, it was found that the introduction of nano-Bi not only accelerates the charge transfer rate at high current density, but also significantly improves the VE and EE of the battery. In addition to the hydrogen evolution problem of metal Bi, the loading amount of metal Bi is also worthy of exploration. Similarly, Yang *et al.* introduced Bi with different loadings on the CF surface by using a high-temperature hydrogen gas thermal reduction strategy.[111] The loading method of Bi is as follows. First, CF is impregnated with the solution of Bi^{3+} and dried, and then high-temperature reduction is carried out under N_2/H_2 and Ar/H_2 respectively to convert Bi^{3+} into Bi and anchor it on the CF surface. Moreover, this work innovatively uses heat treatment to enhance the adhesion between Bi and CF, and improve the stability of Bi. In addition, the researchers compared the effects of different Bi loadings on the electrochemical performance of the electrodes and found that the CF electrodes with 2% Bi loading (based on weight percentage) have the lowest R_{CT}, and the assembled battery can reach 80.9% EE after cycling 300 times at 140 mA cm^{-2}, showing good electrochemical performances. Too high Bi loading will increase the conductive

Table 2 Performance comparison of different carbon-based catalyst modification strategies

Characteristics	Doped substances	P_{max} (mW cm^{-2})	EE		R_{CT}[a] (Ω)	R_{CT}[a] (Ω cm^2)	Ref.
			Cycle number	Current density (mA cm^{-2})	R_{CT}[b] (Ω)	R_{CT}[b] (Ω cm^2)	
0D	C_{76}	—	—		4	—	68
			—	—			
	CDs	—	73%		*ca.* 7	—	69
			1000	150			
1D	CNTs	803.9	82.4%		*ca.* 4	—	71
			550	200	*ca.* 0.2		
	CNTs	—	85.7%		—		72
			50	30			
	CNTs	—	80%		*ca.* 0.3	—	77
			1000	300	*ca.* 0.5		
	CNFs	—	75.4%		—	0.079	82
			1000	320			
	CNFs	1109.5	*ca.* 79%		—	2.46	83
			100	100			
2D	Graphene	*ca.* 325	*ca.* 81%		—		86
			500	80			
	Graphene	1130.09	87.16%		0.66	—	87
			800	100			
	Graphene	1189	*ca.* 83%		1.02	—	89
			500	100	—		
3D	Mesoporous graphene	—	80%		0.94	—	92
			100	100	0.94		
	Vertical graphene	1308.5	83.3%		—	*ca.* 3	93
			750	300			
	CNFs/CNTs	—	*ca.* 85%		—		94
			—	40			
	Nanosheets/CNTs	—	—		10.7	—	98
			—	—	7.74		
	Derived from bamboo	1064.6	85%		0.45	—	100
			1000	120			
	Derived from lotus seed	345	83%		0.047	—	101
			150	100			
	Derived from guanosine	—	*ca.* 87%		*ca.* 4	—	102
			100	100	*ca.* 3		

[a] R_{CT} for VO^{2+}/VO_2^+. [b] R_{CT} for V^{2+}/V^{3+}.

resistance of the CF electrodes, while too low Bi loading cannot effectively improve the catalytic performance of the electrode material. Therefore, a reasonable catalyst loading is the key to optimizing the performance of the material.

To further enhance the modification effect of metallic Bi, researchers have also investigated the influence of the distribution and size of Bi on the surface of carbon electrodes on electrode performance. A uniform distribution of metallic Bi with a reasonable size on the surface of carbon materials can maximize the catalytic performance of Bi. Jiang *et al.* discovered that oxygen-containing functional groups on CF can regulate the size of Bi, promote its even distribution, and exhibit a synergistic catalytic effect with Bi.[112] The synergistic mechanism between oxygen-containing functional groups and Bi is illustrated in Fig. 11a–f, where Fig. 11a–c represent the graphite structures without the introduction of oxygen-containing functional groups, and Fig. 11d–f represent the graphite structures with the introduction of oxygen-containing functional groups (C═O). As shown in Fig. 11d, the introduction of C═O causes C to protrude from the structural plane, effectively activating inert π electrons and enhancing the surface adsorption capacity. Additionally, as shown in Fig. 11f, a large number of electrons are transferred from Bi to the surface with CO groups, indicating that the CO groups have good adsorption properties for Bi. Simultaneously, the CO groups can promote the uniform distribution of electrons across Bi and the carbon substrate, which is beneficial for electrochemical reactions. Under the synergistic effect of oxygen-containing functional groups, small-sized Bi is uniformly distributed in the electrode material, endowing the electrode with excellent ion transport performance. The VRFBs assembled with these electrodes achieve an EE of 92.5% at 80 mA cm^{-2} and 88.4% at 160 mA cm^{-2}, and even maintain an EE of 80.1% at 320 mA cm^{-2}. For metal catalysts, the size effect is an interesting phenomenon, as the same metal catalyst may exhibit significantly different performances depending on its size.[113]

Large-sized and sparse-distributed Bi can limit catalytic performance. Reducing the size of Bi and studying its impact on electrodes is an important research direction in the future. Zhou *et al.* achieved semi-embedding of nano-sized spherical Bi

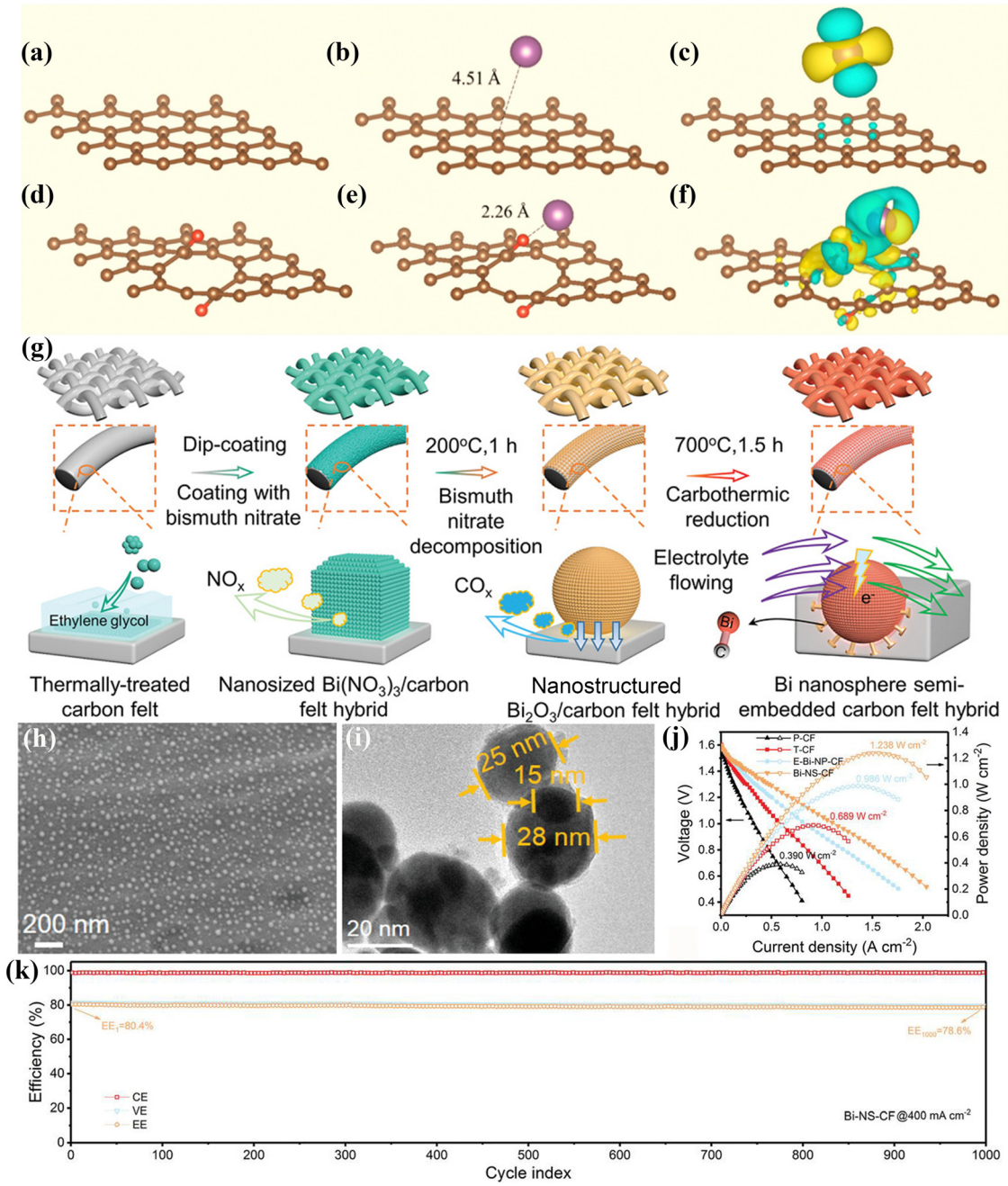

Fig. 11 (a) Original graphite surface. (b) Bi modification of the original graphite. (c) The charge difference plots of Bi modified graphite. (d) Graphite with carbonyl groups. (e) Graphite containing carbonyl groups after Bi modification. (f) The charge difference images of Bi modified graphite with carbonyl groups (the yellow areas indicate electron gain and the blue areas indicate electron loss).[112] Copyright (2019). Elsevier. (g) Flow chart for the preparation of semi-embedded CF in Bi nanospheres. (h) SEM image of Bi-NS-CF. (i) TEM image of Bi-NS-CF. (j) Polarization curves. (k) The assembled battery of the side, peacekeeper.[114] Copyright (2020). Wiley-VCH.

uniformly into CF through carbothermal reduction of bismuth oxide, and assembled it into a Bi-NS-CF electrode, as shown in Fig. 11g–k.[114] This work controls the size of metallic Bi to 25 nm, and the Bi nanospheres are embedded inside the porous CF with high density and dispersion, significantly increasing the active sites on the CF surface. Moreover, the bismuth nanospheres are also bonded to the carbon structures, enabling them to maintain high stability in the flowing electrolyte. The peak power density of the Bi-NS-CF electrode reaches 1238 mW cm^{-2}, with an EE of 78.6% and an EE retention rate of 98.2% after 1000 cycles. Liu *et al.* further reduced the size of Bi to 10 nm and fabricated a uniformly distributed Bi-modified electrode (Bi@TGF) through a polyvinylpyrrolidone-guided method.[115] The precise Bi electrocatalyst not only plays a

crucial role in catalyzing the V^{2+}/V^{3+} redox reactions but also effectively suppresses the hydrogen evolution side reactions. The AVFBs assembled with Bi@TGF demonstrate a peak power density of 1023 mW cm^{-2} and an EE of 81.5% at 200 mA cm^{-2}. Furthermore, the Bi@TGF electrodes exhibit an outstanding stability in a 2500-cycle ultra-long charging–discharging test at 300 mA cm^{-2}, with an EE retention rate of 99.2%. Surprisingly, to further improve the modification effect of metal Bi on the electrodes, Xing *et al.* used N atoms to anchor the metal Bi on GF to form electrodes with Bi–N_4 coordination (Bi SAs/NC@GF), which were applied to VRFBs (1.6 M V^{3+}/VO^{2+} and 3 M H_2SO_4 as the electrolyte).[116] The modification mechanisms are as follows. (i) Bi–N_4 can promote the desolvation of vanadium ions in the electrolyte and reduce the reaction barrier of vanadium ions. The coordination bond of Bi–N_4 promotes the deformation of the vanadium ion structure after solvation with water molecules ($[V(H_2O)_6]^{3+}/[V(H_2O)_6]^{2+}$) and forms $^*Bi[V(H_2O)_5]^{3+}$ with high catalytic activity and stability, thereby improving the performance of VRFBs. (ii) Relying on the inner-sphere reaction mechanism can facilitate charge transfer. During charge transfer, $^*Bi[V(H_2O)_5]^{3+}$ transforms to $^*Bi[V(H_2O)_5]^{2+}$, followed by desorption. Then, HSO_4^- and SO_4^{2-} adsorb around V^{2+} to form coordination bonds, which contribute to facilitating the conversion of V^{3+} to V^{2+} and increase the charge transfer during the reaction. The assembled VRFBs exhibit a peak power density of 990 mW cm^{-2} at 240 mA cm^{-2} and achieve an EE of 80% after 1500 cycles. This work provides a new idea for metal Bi-modified electrodes.

Other metal nanoparticles also show outstanding performance on modified PFFEs. Mehboob *et al.* transformed Sn^{2+} in the electrolyte into Sn nanoparticles and deposited them on CF by *in situ* electrodeposition.[117] Since the deposition potential of Sn^{2+}/Sn is close to the potential of the V^{3+}/V^{2+} reduction reactions, the catalytic efficiency of Sn is greatly improved. When the concentration of Sn^{2+} ions in the electrolyte is 0.01 M, the assembled VRFBs exhibit outstanding performance (77.3% EE at 150 mA cm^{-2}). The addition of Sb^{3+} to the negative electrolyte and its deposition on the GF surface improve the catalytic performance.[118] Under the optimal Sb^{3+} ion concentration of 5 mM, the EE shows a maximum (67.1%) at 120 mA cm^{-2}. Notably, the above-mentioned metal nanoparticles mainly act on the negative electrode of VRFBs, while Ir is often used to improve the performance of the positive electrode of VRFBs because it can reduce the overpotential of the VO^{2+}/VO_2^+ redox reactions in CF electrodes. Cheng *et al.* prepared Ir-modified carbon electrode materials through electrospinning and pyrolysis processes.[119] The VRFBs with these electrodes as the positive electrode show an EE of 75.4% at 150 mA cm^{-2}.

Metal-based catalysts are a type of highly efficient catalyst with high commercial application value. However, side reactions such as hydrogen evolution and high prices still restrict the application of these catalysts. Currently, preparation processes such as deposition strategies and heat treatment are new ways to solve side reactions such as hydrogen evolution, which are expected to expand the application of metal-based catalysts. More importantly, regulating the size and distribution of metal particles, especially Bi, will have a significant improvement in performance, which brings new ideas for the research of high-performance electrodes.

3.2.3 Metal oxide catalysts. Compared with high-cost metal catalysts, cost-effective metal oxides are more favored by researchers and have undergone rapid development in the field of VRFB catalysis. More importantly, the rapid development of metal oxides is also related to their own physicochemical properties. As shown in Fig. 12a, O^{2-} in metal oxides has a good affinity for vanadium ions, which can significantly improve the adsorption of vanadium ions by materials.[120] In addition, when modifying PFFEs, metal oxides will increase the carboxyl and hydroxyl groups in the carbon structure, which will optimize the catalytic performance of PFFEs for the redox reactions of vanadium ions. Currently, common metal oxide catalysts include TiO_2, NiO, WO_3, PbO_2, MoO_3, CeO_2, MnO_2, ZrO_2, *etc.*

TiO_2 is a low-cost, highly hydrophilic, and stable metal oxide in acid solutions. Hsiao *et al.* prepared a TiO_2-modified N-doped GF through a simple one-pot synthesis strategy.[124] The specific TiO_2 loading strategy is as follows. First, GF is impregnated with the Ti-containing solution to make Ti particles load on GF. Then, the product is annealed at high temperature in an N_2 atmosphere for oxidation to form TiO_2 and is stably loaded on GF. Owing to the etching of TiO_2 and doped N atoms, the obtained electrodes exhibit a large SSA and high hydrophilicity, which significantly enhances adsorption and catalytic effects on VO^{2+}/VO_2^+. The assembled battery shows an EE of 77.8% at 160 mA cm^{-2}, which is significantly better than that of untreated GF. Although TiO_2 is stable in acid solutions, a small amount of hydrogen evolution reaction still occurs. Researchers directly grew hydrogen-treated TiO_2 nanorods on GF by a hydrothermal method and used them for VRFB electrodes, as shown in Fig. 12b.[121] Hydrogen-treated TiO_2 not only introduces defects and increases the SSA, but also completely inhibits the hydrogen evolution reaction. Meantime, the direct growth strategy avoids the negative effects such as increased resistance caused by the introduction of binders. The prepared electrodes can effectively catalyze the V^{3+}/V^{2+} reactions, and exhibit high capacity retention and good stability. NiO is an important metal oxide, which can improve the electronic conductivity after combining with the carbon material structure. After the GF electrodes are combined with NiO, the hydrophilicity and SSA of the electrode are significantly improved, and the mass transfer function is also improved, as shown in Fig. 12c.[122] In particular, the electrodes still show an EE of 74.52% at 125 mA cm^{-2} and long cycle stability (300 cycles at 100 mA cm^{-2}). WO_3 is also commonly used to modify CF electrodes to improve the adsorption of vanadium ions on the electrodes. This is mainly due to the multiple valence states of tungsten ions, which help the dissociation of water and the adsorption of a large number of OH^-, thereby promoting the adsorption of vanadium ions on the electrode and improving the catalytic performance. Hosseini *et al.* introduced an N-doped WO_3 catalyst on CF electrodes by hydrothermal reaction

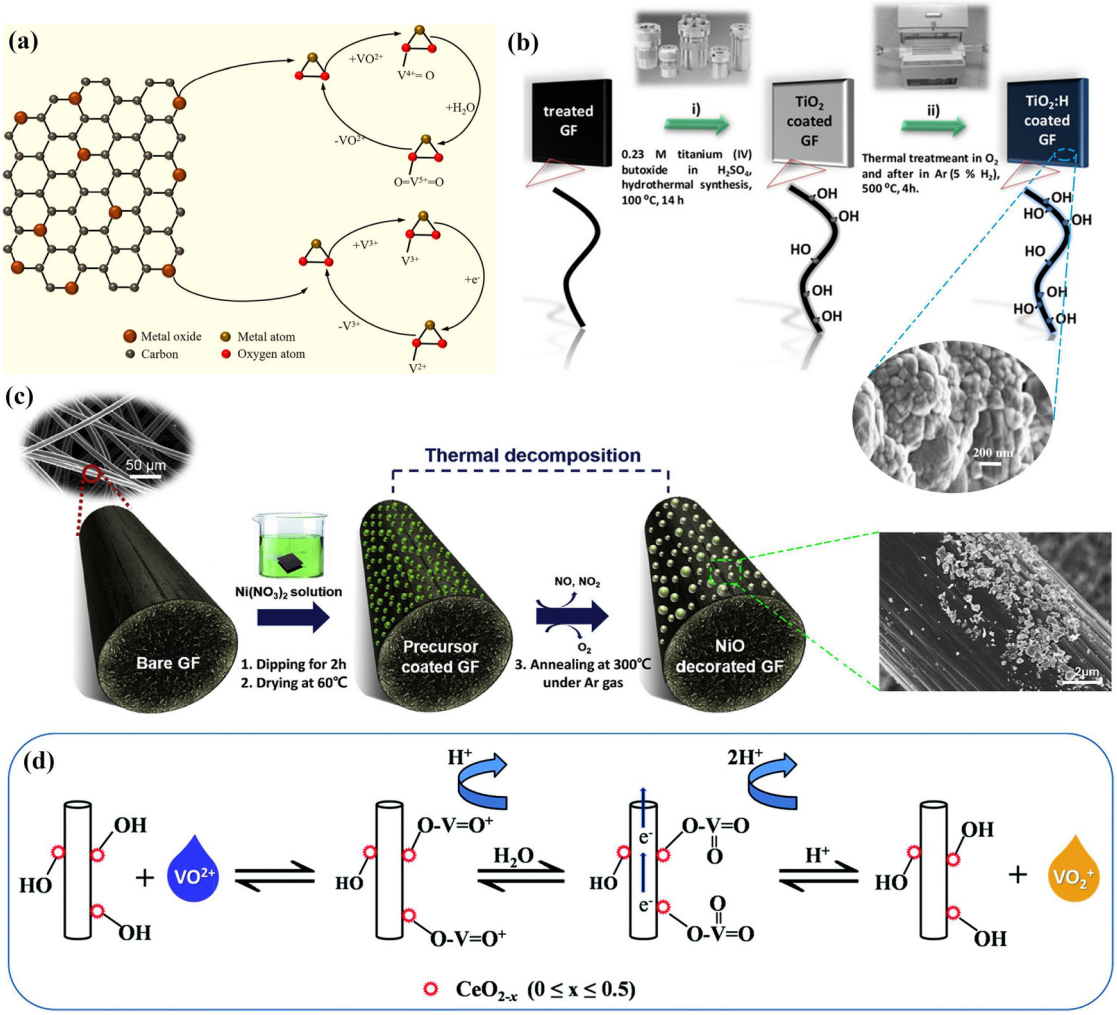

Fig. 12 (a) Catalytic and adsorption mechanism of vanadium ions by metal oxides.[120] Copyright (2021). ACS Publications. (b) Preparation steps of GF electrodes modified by TiO_2 and defects.[121] Copyright (2017). Chemistry Europe. (c) Flow chart of the preparation of the NiO-modified GF electrode.[122] Copyright (2018). Elsevier. (d) Diagrammatic sketch of the catalytic effect of CeO_2 on vanadium ions.[123] Copyright (2014). Royal Society of Chemistry.

and used it for the redox reaction of VO^{2+}/VO_2^+ in VRFB positive electrode catalysis.[125] Owing to the synergy of N atom doping and WO_3 catalyst, the prepared electrodes not only achieve high reversibility of the VO^{2+}/VO_2^+ reactions at high current density, but also significantly reduce the R_{CT} (from 76.18 to 13 Ω). In addition, the electrodes achieve 51% electrolyte utilization and 70% EE at 200 mA cm^{-2}. PbO_2 has the characteristics of cheap cost, high hydrogen evolution potential, and strong stability, which make it an efficient electrocatalyst. Wu *et al.* prepared PbO_2 by pulsed electrodeposition and introduced it to GF for VRFBs.[126] PbO_2 is uniformly dispersed on the GF surface, which can catalyze the redox reaction of vanadium ions and significantly reduce the R_{CT} on the electrode surface. The assembled battery shows an EE of 82% at a current density of 70 mA cm^{-2}. However, PbO_2 is a toxic substance, which to some extent limits the large-scale application of PbO_2.

Mo has multiple states and oxides, which make MoO_3 easily convertible to other oxidation states, thereby endowing MoO_3 with high electrochemical activity. Xie *et al.* deposited MoO_3 nanoparticles on GF by an impregnation process and used them for catalyzing the VO^{2+}/VO_2^+ redox reactions at the positive electrodes of VRFBs.[127] Due to the excellent electrochemical properties of MoO_3, the prepared battery provided 80% electrolyte utilization at 100 mA cm^{-2} and exhibited 65.34% EE at ultra-high current density (250 mA cm^{-2}). CeO_2 is a low-cost and highly stable electrocatalyst with a fluorite cubic structure with a space group of *Fm*3*m*, where each Ce ion is coordinated with eight oxygens. The electronic structure of Ce ($[Xe]4f^15d^16s^2$) makes it easier to achieve charge transfer between the 4-valent and 3-valent states, which helps to improve conductivity.[128] Specifically, the electrocatalytic mechanisms of CeO_2 are shown in Fig. 12d, accompanied by the reactions of Equations (1) and (2).[123] Firstly, the conversion of Ce^{4+} and Ce^{3+} generates oxygen vacancies that are beneficial for the transport and binding of vanadium ions, as shown in Equation (1). Subsequently, at a low potential, the active sites of Ce^{3+} are occupied by OH^- in the solution, resulting in the formation of H^+, as shown in Equation (2). When VO_2^+ in the

solution migrates towards the electrode, it undergoes a charge exchange with the electrode and is converted into VO_2^+. During this process, electron transfer occurs, and the generated VO_2^+ diffuses back into the solution. It is worth noting that the OH^- groups on CeO_2 can significantly enhance the electrocatalytic activity of CeO_2. Zhou *et al.* loaded CeO_2 nanoparticles on GF by a precipitation method and used them for catalyzing the VO^{2+}/VO_2^+ reaction at the positive electrodes of VRFBs (CeO_2/GF).[123] The specific precipitation method is as follows. GF is impregnated with a Ce^{4+} solution for the adsorption of Ce^{4+}. Then, ammonia water is added to adjust the pH to 8, thus forming the $Ce(OH)_3$ precipitate. The GF loaded with the $Ce(OH)_3$ precipitate is placed in a tube furnace and calcined at a high temperature to obtain CeO_2/GF. The introduction of CeO_2 significantly improves the electrocatalytic activity and hydrophilicity of the electrode. After balancing the electrocatalytic effect and electrical conductance loss, it was found that 0.2 wt% CeO_2/GF had the optimal EE (64.7% at 200 mA cm^{-2}) and excellent cycling stability. To further enhance the catalytic activity of CeO_2, Bayeh *et al.* deposited hydrogen-annealed CeO_2 nanowires on GF by a hydrothermal method and used them as electrodes for VRFBs.[129] The hydrogen annealing process significantly enhanced the defects of CeO_2 nanowires and improved their electrocatalytic performance. In addition, the uniform distribution of CeO_2 nanowires on the GF surface also enhanced the cycling stability of the electrode. The assembled VRFBs showed the best EE of 64.75% at 160 mA cm^{-2}, and there was no significant attenuation in EE after 100 cycles at 80 mA cm^{-2}.

$$CeO_2 \leftrightarrow CeO_{2-x} + (x/2)O_2\ (0 \le x \le 0.5) \quad (1)$$

$$CeO_{2-x} + H_2O \rightarrow CeO_{2-x} - OH + H^+ + e^- \quad (2)$$

To improve the catalytic performance of metal oxide materials, a new type of metal–organic framework (MOF) method has been proposed. The MOF strategy is a preparation method of materials with porous structures formed by self-assembly of metal ions or metal clusters with organic ligands through coordination bonds. The materials prepared by the MOF method not only have a rich porous structure and a large SSA, but also a solid framework structure that can provide excellent stability for the material. Chen *et al.* first synthesized a MnO@C catalyst by the MOF method and used it to catalyze the redox reaction of the vanadium ion.[130] Under the electron microscope, the prepared MnO@C has a small size and abundant oxygen-containing functional groups. The assembled battery shows great application potential in terms of both electrochemical performance and cost, being significantly superior to the battery assembled with the original CF electrode. Jiang *et al.* loaded the MOF-derived ZrO_2@C catalyst on GF and used it to improve the catalytic performance of VRFBs, as shown in Fig. 13.[131] The special MOF preparation strategy enables the ZrO_2@C catalyst to grow uniformly *in situ* on GF, ensuring good dispersion of the catalyst and helping to improve the stability of VRFBs. Owing to the porous structures constructed by the MOF and the large SSA of the ZrO_2@C catalyst, the battery can maintain 75.2 and 62.4% EE at 200 and 300 mA cm^{-2}, respectively. In addition, after 500 cycles at 150 mA cm^{-2}, the EE of the battery does not show obvious attenuation, demonstrating good cycling stability. The MOF strategy provides a new method for improving metal oxide catalysts and has positive reference significance.

Metal oxide catalysts are widely used to modify CF electrodes due to low cost and good catalytic efficiency. However, metal oxide catalysts still have problems such as high resistance, strong toxicity and unstable binding with electrodes, which will affect the practical application of these catalysts.[132,133] Some specific strategies are expected to improve these problems. For example, safety assessment systems have been introduced to control and reduce the environmental impact of such catalysts, while preparation processes have been improved, such as better immobilization of such catalysts to electrodes using *in situ* growth strategies, deep burial methods, or MOF methods to improve efficiency. In addition, among the above strategies, we believe that metal oxides improved by the MOF strategy, such as MnO_2 and ZrO_2, exhibit advantages such as good energy efficiency and excellent stability, and are highly promising catalysts. This is closely related to their large specific surface area, abundant defect sites, and stable porous structure.

3.2.4 Metal carbide catalysts. Metal carbides, like metal oxides, are commonly used catalysts in VRFBs. Metal carbide catalysts have high stability, acid resistance, high mechanical strength, and other characteristics, and have been widely applied in VRFBs in recent years. Currently, in the field of VRFB catalysis, the reported metal carbides mainly include TiC, WC, Mo_2C, *etc.* Ultrafine TiC nanoparticles are transition metal carbide nanoparticles with high conductivity and excellent catalytic activity, which can provide highly catalytic active centers for the redox reaction of V^{3+}/V^{2+}. Wei *et al.* introduced TiC electrocatalysts onto carbon materials by dip coating and used them to catalyze the redox reaction of V^{3+}/V^{2+}.[134] It was detected that the carbon materials modified by TiC have the lowest charging platform, the highest discharging platform, and the largest capacity, which is because TiC can efficiently catalyze the redox reaction of V^{3+}/V^{2+}. The assembled VRFBs achieved an EE of 80.7% at 100 mA cm^{-2}, low R_{CT}, and excellent stability. However, these catalysts are often unstable when combined with electrodes, especially in the face of disturbances from flowing electrolytes. To improve this situation, Wei *et al.* uniformly embedded Ti and O atoms of TiO_2 crystals on the CF surface, and deposited TiC catalysts protected by wormhole-like nanopores on the surface, as shown in Fig. 14.[135] The loading method of TiC is mainly described as follows. The CF is impregnated with $TiCl_4$ and dried. During this process, $TiCl_4$ will hydrolyze to form TiO_2 and precipitate onto the structure of CF. Then, the product is placed in a tube furnace. Under the protection of N_2 at 1300 °C, TiO_2 will corrode and react with the CF substrate to generate TiC and deposit in the pore structure. The catalyst deposited on the CF surface is neither easily dispersed by the electrolyte nor hinders the flow of the electrolyte. At the same time, the formed wormhole-like nanopores not only protect the TiC catalyst and improve the catalytic

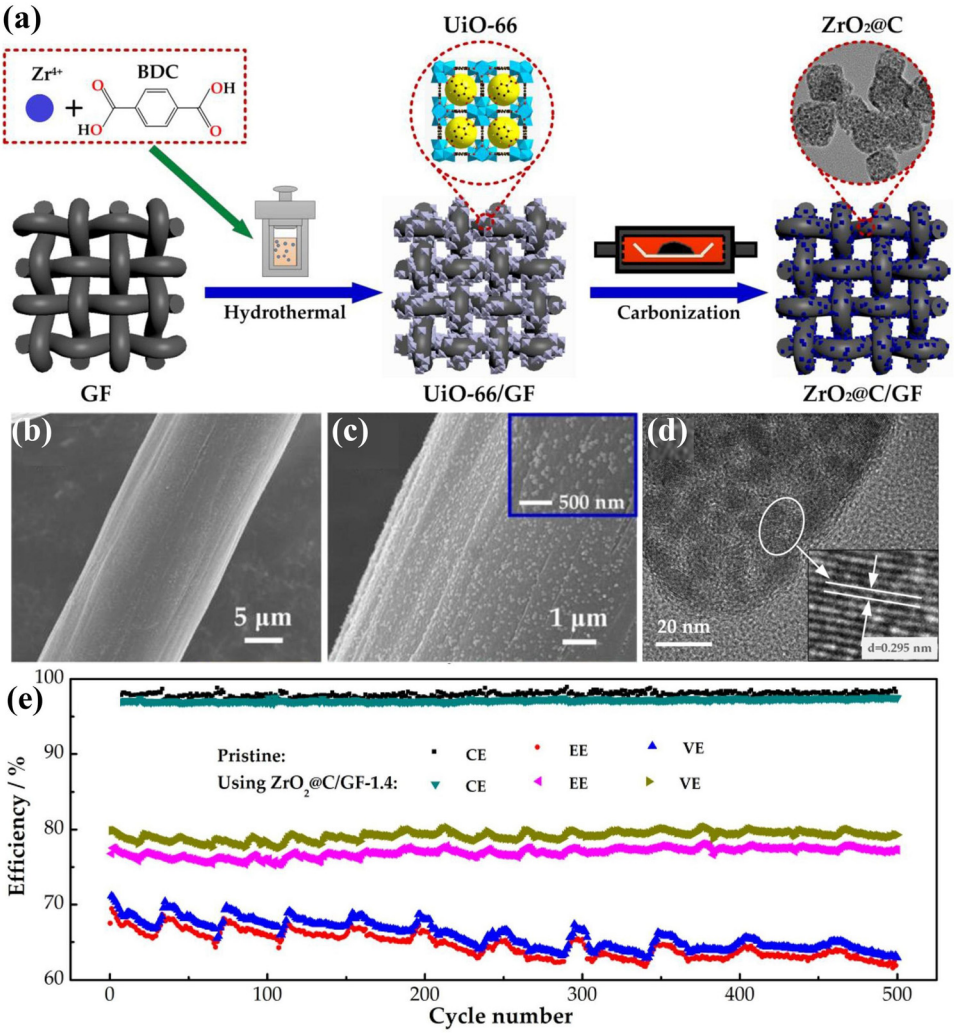

Fig. 13 (a) Preparation flowchart, (b) and (c) SEM images, (d) HRTEM image, and (e) CE, VE and EE at 150 mA cm^{-2} for 500 cycles of ZrO_2@C nanoparticle-modified GF electrodes.[131] Copyright (2021). Elsevier.

efficiency, but also make the distribution of TiC uniform and avoid the accumulation of the catalyst. In addition, the VRFBs assembled with these CF electrodes have an EE of 85.2% and an electrolyte utilization rate of 82.7% at 200 mA cm^{-2}; even at 300 mA cm^{-2}, the EE and electrolyte utilization rate can still be maintained at 80.8% and 72.6%, respectively. It is worth noting that these batteries can still stably show an EE of more than 80% in the cycle performance test. This strategy provides a simple and efficient strategy for embedding catalysts into CF, which is beneficial for subsequent in-depth research.

The high stability of WC in acidic environments is the key to its popularity among researchers. Cheng *et al.* used ammonium tungstate as the tungsten source to introduce WC into CNFs through electrospinning technology and *in situ* carbothermal reaction, which was used to catalyze the redox reaction of vanadium ions.[136] WC is firmly embedded in the CNFs, avoiding the introduction of binders and enhancing the bonding degree between WC and the materials. Benefiting from the high stability and high catalytic activity of WC, the prepared electrode has no obvious hydrogen evolution side reaction, and exhibits a high EE (61.1% at 150 mA cm^{-2}) and electrochemical stability. The preparation process of WC often adopts high-temperature annealing processes that limit the performance of the material, thus restricting the application of WC catalysts. Wodaje *et al.* proposed a two-step strategy to introduce N-doped WC nanowires onto GF.[137] The introduction of N doping changes the charge density on the surface of the material, promoting the adsorption and transport of vanadium ions. The nanowire structures of WC also provide a large SSA for the attachment of active sites, which promote the redox reaction of vanadium ions. Under the synergistic effect of N doping and the WC nanowire structures, the prepared battery exhibited an optimal EE of 74.8% at 100 mA cm^{-2} and excellent cycle stability.

Metal carbides are substances with acid resistance and high mechanical strength, and they have only gradually attracted the attention of researchers in recent years. However, the

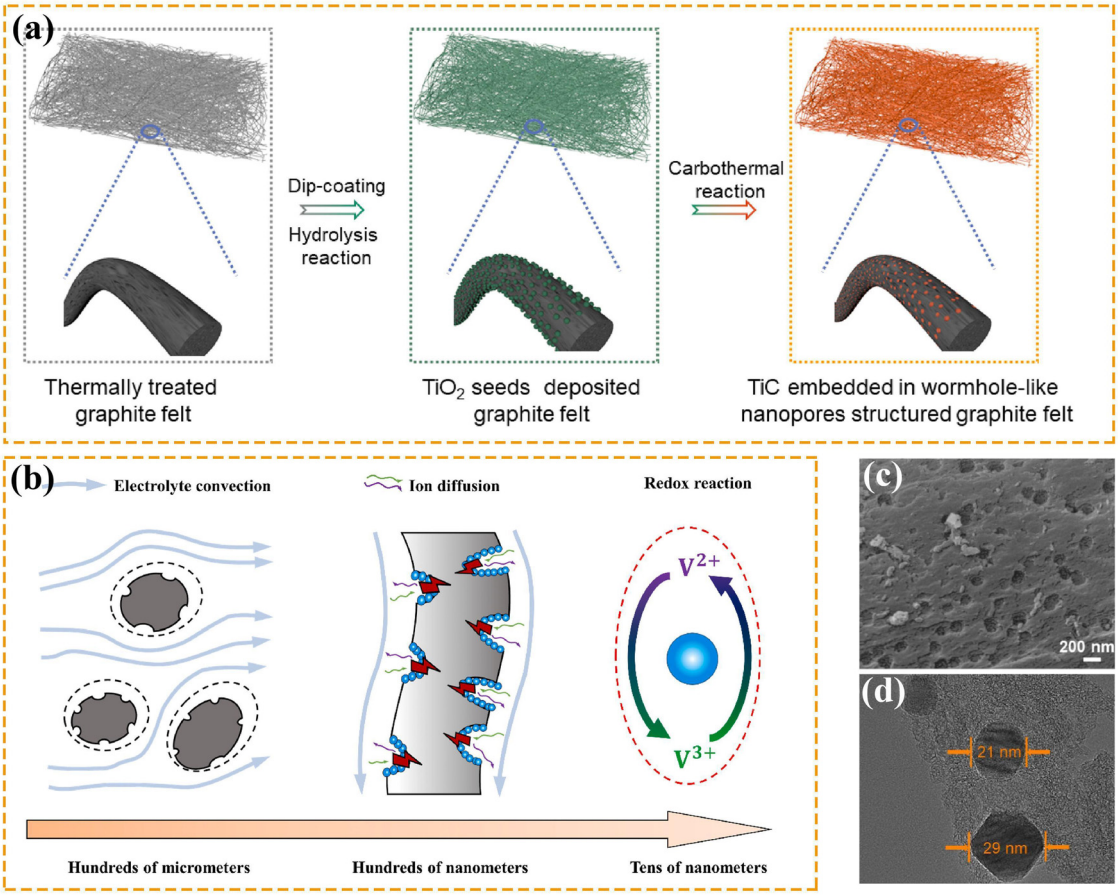

Fig. 14 (a) Flow diagram of TiC in wormhole-like nanopores embedded in the surface of CF. (b) Schematic diagram of the battery electrode surface. (c) SEM image of TiC-WN-GF. (d) TEM image of TiC-WN-GF.[135] Copyright (2023). Elsevier.

preparation process of metal carbides is highly dependent on extreme conditions such as high temperature and high pressure, which have extremely high equipment requirements, limiting the large-scale application of these catalysts. At the same time, some metal carbide raw materials are scarce or difficult to obtain, which also increases the preparation cost and difficulty. Exploring new carbide materials and simple processes is the key to promoting the future development of such metal carbides. In addition, among the metal carbides introduced above, we believe that TiC deposited in carbon nanopores is an outstanding catalyst. It has a relatively low cost compared to other metal carbides and can operate under various current densities, demonstrating excellent performance.

3.2.5 Other types of catalysts. In addition to the aforementioned common catalysts, some catalysts with specific physicochemical properties have also come into the view of researchers. B_4C is an atomic crystal with a structure similar to that of diamond, in which each C atom forms a tetrahedral structure with four B atoms, and each B atom forms a triangular pyramid structure with three C atoms. This particularity endows B_4C with outstanding physicochemical performance, such as high stability and excellent mechanical strength. Jiang *et al.* prepared a highly active and bifunctional GF electrode uniformly modified with B_4C for use in VRFBs.[138] The specific strategy for loading B_4C onto CF is as follows. Immerse the GF in a solution rich in B_4C, and then use the dip–withdraw–dry process to firmly precipitate B_4C onto the GF. Notably, in the special electronic structure arrangement of B_4C, due to the electronegativity of C being greater than that of B, the electrons tend to be distributed near the central C atom. The uneven electron distribution in B_4C has a positive promoting effect on the redox reaction, which helps catalyze vanadium ions and improve the overall performance of VRFBs. At the same time, the uniformly distributed B_4C can significantly enhance the active SSA of the electrode and further optimize the performance of the electrode. It was detected that the electrode can catalyze the V^{2+}/V^{3+} and VO^{2+}/VO_2^{+} reactions, which exhibit bifunctional effects. In addition, when the loading amount of B_4C nanoparticles reaches 2 mg cm^{-2}, the VRFBs exhibit outstanding electrochemical performance. The EE of VRFBs is 88.9% and 80.0% at 80 mA cm^{-2} and 160 mA cm^{-2}, respectively, and it even reaches 72.0% at 240 mA cm^{-2} and 63.8% at 320 mA cm^{-2}, without significant attenuation after 200 cycles at 160 mA cm^{-2}. These results indicate that the battery has excellent rate performance and stability, which has great application value.

C_3N_4 is a typical 2D conjugated polymer material that is used for CF modification owing to its excellent physicochemical properties, high nitrogen content, and unique electronic structure. Huang *et al.* first used the new material C_3N_4 to modify CF electrodes and catalyze the redox reaction of vanadium ions in VRFBs.[139] The way of loading C_3N_4 on CF is as follows. The CF is impregnated with a solution rich in melamine and dried, and then it is placed in an Ar atmosphere and calcined at 400 °C for 4 hours, thus obtaining the CF with C_3N_4 anchored. Moreover, C_3N_4 uniformly wraps around CF, and its wrinkled structure significantly increases the SSA of CF (from 3.088 to 6.835 $m^2\ g^{-1}$), expanding the attachment of active sites. Moreover, in the electronic structure of C_3N_4, C atoms and N atoms possess lone electron pairs in their p orbitals, which can interact to form P-conjugated structures similar to six-membered rings, thereby forming a conjugated system. This system structure can significantly improve the reversibility of the redox reaction and the overall electrochemical performance. Owing to the introduction of the C_3N_4 catalyst, the prepared electrode maintained an EE of 85% at 50 mA cm^{-2}, which is 9.1% higher than that of commercial CF. In addition, the electrode also had a large capacity and good cycle stability. The emergence of C_3N_4 materials provides new ideas for the development of high-performance VRFBs. In addition, some novel catalysts like TiB_2, owing to their special electron-deficient site structures, can effectively alleviate the concentration polarization in the negative electrode region of VRFBs resulting from the sluggish kinetics of V^{2+}/V^{3+}. Huang *et al.* introduced the TiB_2 catalyst with electron-deficient sites onto the electrodes of VRFBs to accelerate electron transfer.[140] The oxidation reaction of V^{2+}/V^{3+} has a high Tafel slope and a large overpotential during the oxidation process, which limits the performance of VRFBs to some extent. The TiB_2 catalyst with an electron-deficient structure can promote the electron transfer in the oxidation reaction of V^{2+}/V^{3+} and enhance the corresponding reaction kinetics. The faster reaction kinetics not only optimizes the performance of VRFBs to a certain extent but also promotes the conversion between V^{2+} and V^{3+}, avoiding the concentration polarization caused by untimely conversion.

These special catalyst materials have gradually been applied in the field of VRFBs in recent years. Although these catalysts show attractive effects in modifying PFFEs, the demanding preparation process restricts their development. New and simple preparation processes are important driving forces for the development of such materials. Preparing and loading these catalysts at low cost, simply, and efficiently on CF/GF is an important research direction in the future. Among the other types of catalysts mentioned above, we consider the TiB_2 catalyst to be highly interesting and valuable. This is mainly because the TiB_2 catalyst utilizes its own electron-deficient structure characteristics to promote the conversion of vanadium species. It not only reduces the concentration polarization but also significantly enhances the catalytic performance of TiB_2, which provides a novel perspective for subsequent catalyst design. Utilizing the unique structure of materials to promote the improvement of electrochemical performance represents a highly promising development path in the future. In addition, we summarize and compare the specific properties of the above catalysts in Table 3 to provide reference for subsequent studies.

To significantly enhance the reference value of this work, after in-depth research on the above various strategies, we have carefully selected the key strategies that are highly promising to promote the successful transition of the PFFEs from laboratory research to industrial-scale applications. In the macroscopic design, the optimization of the electrode shape and thickness is crucial for industrial production and application. Among them, the trapezoidal electrode shape can effectively alleviate the concentration polarization phenomenon and is easy to implement in industrial production, having significant advantages. In terms of thickness selection, considering both cost and performance, a thick electrode is more suitable for a single-channel flow field, while a thin electrode is preferred for a multi-channel flow field. In terms of intrinsic treatment for microscopic design, the multi-atom co-doping strategy has attracted much attention. In particular, the preparation of multi-atom-doped hierarchical porous carbon materials using the molten salt system has outstanding advantages. This method has a simple process and can effectively enhance the synergistic effect among multiple atoms, thus greatly improving the material performance and showing great potential in the industrialization process. In the aspect of introducing catalysts, the 3D graphene-based carbon catalyst has achieved fruitful results in many laboratory studies and has become one of the most promising catalysts, which deserves special attention in future industrial applications. Among metal catalysts, Bi is a commonly used choice. Nano-sized bismuth metal uniformly and stably distributed on the electrode structure can endow the electrode material with excellent electrochemical properties, making it a highly promising catalyst material. Notably, the development of metal oxides is limited due to problems such as low conductivity and unstable binding. However, the low cost and ease of synthesis of metal oxides prompt researchers to continuously optimize their performance. Some efficient synthesis strategies such as the MOF strategy may be the key to breaking through the bottleneck of metal oxides. Moreover, for metal carbides, TiC is considered as an ideal choice due to its excellent performance in the preparation process and cost control. Some novel ideas for catalyst preparation are also highly valuable. For example, taking advantage of the electron-deficient structure characteristics of the TiB_2 catalyst to promote the conversion of vanadium substances not only reduces the concentration polarization but also significantly enhances the catalytic performance of TiB_2. In conclusion, these strategies are determined after a comprehensive consideration of cost and performance, and the detailed results are listed in Table 4. In future electrode structure design, it can be considered to combine the most effective path of each modification strategy, thus achieving better electrochemical performances. For example, 3D graphene doped with heterogeneous atoms is grown on the surface of a trapezoidal electrode, and then Bi nanoparticles are

Table 3 Comparison of the performance of the introduced catalyst modification strategies

Optimized strategies	Doped substances	P_{max} (mW cm^{-2})	EE		R_{CT}[a] (Ω)	R_{CT}[a] (Ω cm^2)	Ref.
			Cycle number	Current density (mA cm^{-2})	R_{CT}[b] (Ω)	R_{CT}[b] (Ω cm^2)	
Metal-based catalysts	Bi	1238	78.6%		—	—	114
			1000	400	0.08		
	Bi	—	80.9%		—	—	111
			300	140	20		
	Bi	—	80.1%		—		112
			200	320			
	Bi	1023	*ca.* 71.43%		—		115
			2500	300			
	Bi	990	80%		*ca.* 0.1		116
			1500	240			
	Sn	—	77.3%		—	—	117
			—	150	14.6		
	Sb	—	*ca.* 78%		—		118
			53	60			
	Ir	—	*ca.* 64%		0.6	—	119
			—	150	—		
Metal oxide catalysts	TiO_2	—	83.3%		64	—	124
			—	100			
	TiO_2	—	66.1%		—		121
			100	150			
	NiO	—	78.5%		5.4	—	122
			300	100	2.8		
	WO_3	350	65.4%		13	—	125
			—	200			
	PbO_2	—	*ca.* 87.5%		7.2	—	126
			30	50			
	MoO_3	—	76.33%		1.6	—	127
			50	100	—		
	CeO_2	—	*ca.* 76%		78.3	—	129
			100	80	—		
	CeO_2	—	74%		—		123
			100	100			
	MnO (MOF)	—	*ca.* 73%		*ca.* 0.25	—	130
			300	100	—		
	ZrO_2 (MOF)	—	*ca.* 77%		4.8	—	131
			500	150	4.9		
Metal carbide catalysts	TiC	—	*ca.* 84%		—	—	134
			30	50	1.6		
	TiC	—	*ca.* 80%		—	—	135
			300	300	*ca.* 5		
	WC	—	82.5%		15.7	—	136
			50	50	23.7		
	WC	—	74.5%		6.3	—	137
			100	100			
Other types of catalysts	B_4C	—	*ca.* 69%		—	2.14	138
			200	160			
	C_3N_4	—	*ca.* 84%		23.1	—	139
			25	50			
	TiB_2		74.2%		4.66		140
			300	150			

[a] R_{CT} for VO^{2+}/VO_2^+. [b] R_{CT} for V^{2+}/V^{3+}.

deposited on the graphene surface. Optimizing the growth and deposition process of 3D graphene and Bi nanoparticles is expected to endow the electrode with higher power density and EE.

4. Summary and outlook

VRFBs, which possess characteristics such as intrinsic safety, long lifespan, flexible energy storage duration, and no geographical limitations, are considered as the most promising battery device for large-scale and long-duration energy storage. As a crucial component of the VRFBs, the performance of the PFFEs affects the EE and power density of the battery, thereby determining the overall performance of the battery. However, the traditional untreated PFFEs have low hydrophilicity and poor electrochemical activity, resulting in significant overpotentials during the operation of VRFBs, hindering the redox reactions, and restricting the EE and power density. Therefore,

Table 4 The most effective method in each modification strategy for PFFEs

Optimized strategies	Doped substances or improved topography		P_{max} (mW cm^{-2})	EE		R_{CT}[a] (Ω cm^2)		Ref.
				Cycle number	Current density (mA cm^{-2})	R_{CT} (Ω)	R_{CT}[b] (Ω cm^2)	
Trapezoidal electrode shape	—	—	—	85.6%		Reduce concentration polarization		12
				—	80			
Heteroatom doping	LiCl, KCl, $KClO_3$, NH_4Cl	N, O	—	75.9%		—	*ca.* 5	31
				140	260		*ca.* 5	
Layered porous structure	ZnO etching	N, O	—	81.9%		—	0.068	34
				320	500		0.068	
Introduce catalyst	3D Vertical graphene	N	1308.5	83.3%		*ca.* 3	—	93
				750	300			
	Bi	—	1238	78.6%		—	—	114
				1000	400	0.08		
	ZrO_2 (MOF)	—	—	*ca.* 77%		4.8	—	131
				500	150	4.9		
	TiC	—	—	*ca.* 80%		—	—	135
				300	300	*ca.* 5		
	TiB_2		—	74.2		4.66	—	140
				300	150			

[a] R_{CT} for VO^{2+}/VO_2^+. [b] R_{CT} for V^{2+}/V^{3+}.

modifying and optimizing the PFFEs is essential to improve their adsorption and catalytic properties towards vanadium ions, thereby enhancing the performance of VRFBs and promoting their large-scale application. Therefore, based on the micro and macro perspectives, this review focuses on the advantages and disadvantages of strategies for improving the design of PFFEs and the corresponding mechanisms, and summarizes the promising modification strategies.

However, in practical production applications, not all modification strategies are applicable to industrialized production. We believe that the prerequisites for the PFFE modification strategy to meet industrialized production are that the process is simple, the performance is excellent, and the cost performance is high. In microstructure design, intrinsic treatment is a simple and convenient process, which is a commonly used optimization strategy in industry, such as heat treatment and pickling, and the performance of optimized PFFEs is relatively excellent. Currently, common processes such as heat treatment and pickling used in actual production only introduce oxygen-containing functional groups into the PFFEs, and there are certain limitations on the optimization effect of PFFE performance. In subsequent production, not only diversified functional groups can be introduced, but also defects and vacancies can be constructed on the PFFE surface to improve the SSA of the material. These measures can significantly improve the cost performance of intrinsic treatment. In addition, the modification strategies of introducing catalysts have a more complex process, and the success rate and efficiency of the introduced catalyst are low. Although this modification strategy can greatly improve the performance of PFFEs, it is difficult to be widely applied in actual production and life due to its low-cost performance. Secondly, in the macrostructure design strategy, it is necessary to optimize the compression ratio, shape, thickness, and flow field of the electrode, with the help of the data model. With the support of big data models, these strategies can adjust PFFE parameters for different situations, which can greatly meet the different needs of the market for PFFEs. At the same time, these strategies are simple and effective, making them excellent modification options. It is worth noting that grooming strategies can be combined in a variety of ways, and the effect on improving the PFFE performance will also have a multiplier effect. Therefore, we believe that not only the structures of PFFEs should be controlled at the micro level, but also the PFFE parameters should be designed by combining the big data model at the macro level. Only such a diversified modification mode can maximize the modification effect and is expected to be applied in actual production. Battery stack costs account for about 24% of VRFBs' component costs based on the calculation of a 4 h energy storage duration. As an important battery stack component, the cost and performance of PFFEs directly determine the cost and performance of the stack. Therefore, adopting reasonable PFFE modification strategies can effectively reduce the cost of the design of PFFEs and improve their performance. This is critical for improving the cost performance of VRFBs and enhancing their value for business applications. In addition, based on the vigorous development of current technology, this review also looks forward to the future development trend of PFFEs.

(i) In-depth analysis of the structure–activity relationship and intrinsic mechanisms of PFFEs using novel *in situ* characterization methods. It is well-known that the electrochemical reaction mechanisms are different at the interfaces of the positive electrodes and the electrolyte and the negative electrodes and the electrolyte in flow batteries. Revealing the influence of electrode structural modification on the electrochemical reaction mechanisms at the interfaces of the positive electrodes and the electrolyte and the negative electrodes and the electrolyte is helpful for the differentiated structure design of PFFEs. This should be of concern in future research. Revealing the mechanisms requires advanced *in situ* characterization techniques that can monitor the electrochemical reaction process. Some advanced *in situ* characterization methods, such as *in situ*

optical microscopy, *in situ* differential electrochemical mass spectrometry, *in situ* Raman spectra, and *in situ* infrared nano spectroscopy, can be utilized to monitor the dynamic evolution of microstructures, electronic structures, composition, and phase of the materials during the electrochemical reaction process, which can provide important information on the phase, composition transition process, and material failure mechanism of bulk electrode materials.[141,142] These characterization techniques can be considered to reveal the reaction mechanisms at the electrode–electrolyte interfaces in the flow batteries.

(ii) Introducing high-entropy alloy catalysts on the PFFEs. In recent years, high-entropy alloys composed of five or more elements with equal or roughly equal atomic ratios have been favored by researchers, because of their large multi-element composition space and unique high-entropy hybrid structure, and have been widely used in the field of catalysts and batteries. The multi-element composition of high-entropy alloy catalysts with low cost, high activity, and high stability often brings unexpected cocktail effects. The presence of multiple elements will produce a synergistic effect, which not only provides more active sites for PFFEs and regulates the electronic structure of the materials, but also is expected to catalyze the redox reaction of the positive and negative electrodes and inhibit the side reactions.

(iii) Adopting new preparation technologies. In recent years, several advanced micro-nano fabrication techniques have the potential to bring breakthroughs in the field of PFFEs. These new preparation technologies include laser processing, 3D printing, and Joule heating-based ultra-fast synthesis with its derived methods such as high-temperature shock, extreme thermal treatment, and magnetic induction heating. They offer advantages on the micro and macro structural design of PFFEs. Laser processing can effectively and rapidly regulate the macro structure of PFFEs with high precision. 3D printing has the potential to prepare PFFEs in a fast way, and modulate their surface microstructure with the co-formation of catalysts. Joule heating-based ultra-fast synthesis with its derived methods possesses advantages in the preparation of catalysts such as rapid heating, simple processing, and low cost while also enabling precise control over the heating rate and environmental conditions to modulate the catalyst microstructure of the surface of PFFEs. Compared to traditional heating methods, the catalyst materials synthesized using Joule heating-based ultra-fast synthesis often exhibit remarkable electrochemical properties, including higher electrochemical catalytic activity and more excellent stability. The application of these novel techniques in the fabrication of PFFEs has potential to lead to cost reduction and performance enhancement, thus promoting the widespread use of PFFEs.

(iv) Empower PFFEs with artificial intelligence (AI). At present, AI is promoting the revolutionary upgrading of the industry, and using AI to empower electrodes is the core competitiveness of the next generation of electrodes. AI-empowered electrodes are to realize dataization, intelligence, and integration of electrodes. Dataization refers to the use of machine learning and database to establish the mapping relationship between material properties and characteristic process parameters, use this mapping relationship to predict the electrode performance, and then guide the forming process design. Intelligence refers to the integration of cross-scale calculation methods across atomic, microscopic and macroscopic scales, through the combination of computational simulations, theoretical models, and experimental tools at multiple levels, which is applied to independently design electrode materials. Integration refers to the fully automated and integrated design of electrodes, the integration of stacks, and the assembly of batteries to reduce errors between components. Empowering electrodes with AI is an important direction for future development.

In summary, the modification of PFFEs is an effective strategy to improve the performance of VRFBs and can significantly enhance the commercial value of VRFBs. Achieving the large-scale, low-cost, and high-performance development of PFFEs is an important direction for future research.

Author contributions

H. Hu collected the data and drafted the manuscript. M. Han provided the conception and guided H. Hu to complete the initial manuscript and revise it. J. Liu, K. Zheng, Z. Zou, Y. Mu, F. Yu, W. Li, L. Wei, and L. Zeng revised the manuscript. T. Zhao supervised the work, obtained the funds, and revised the manuscript.

Data availability

No primary research results, software or code have been included and no new data were generated or analyzed as part of this review.

Conflicts of interest

The authors declare no conflict of interest.

Acknowledgements

This work was financially supported by the Guangdong Major Project of Basic and Applied Basic Research (2023B0303000002), Shenzhen Key Laboratory of Advanced Energy Storage (no. ZDSYS20220401141000001), High level of special funds (G03034K001), and Special Funds for the Cultivation of Guangdong College Students' Scientific and Technological Innovation (''Climbing Program'' Special Funds). pdjh2025c10810, pdjh2025c10801.

References

1 G. Ji, L. He, T. Wu and G. Cui, *Appl. Energy*, 2025, **377**, 124538.

2 L. Pan, Z. Guo, H. Li, Y. Wang, H. Rao, Q. Jian, J. Sun, J. Ren, Z. Wang, B. Liu, M. Han, Y. Li, X. Fan, W. Li and L. Wei, *ChemElectroChem*, 2024, **11**, e202400460.
3 H. Hu, M. Han, J. Liu, K. Zheng, Y. Mu, Z. Zou, F. Yu, W. Li and T. Zhao, *Future Batteries*, 2024, **4**, 100008.
4 R.-Z. Zhang, M.-Y. Lu, W.-W. Yang, L.-X. Liang and Q. Xu, *J. Energy Storage*, 2024, **90**, 111768.
5 W. Jiang, F. Jiang, J. Zhang, F. Yang, L. Liu and M. Hu, *J. Energy Storage*, 2024, **80**, 110274.
6 X. Zhang, X. Ye, S. Huang and X. Zhou, *ACS Appl. Mater. Interfaces*, 2021, **13**, 37111–37122.
7 T. Cheng, S. Qi, Y. Jiang, L. Wang, Q. Zhu, J. Zhu, L. Dai and Z. He, *Small*, 2024, **20**, 2400496.
8 J. Charvát, P. Mazúr, J. Dundálek, J. Pocedič, J. Vrána, J. Mrlík, J. Kosek and S. Dinter, *J. Energy Storage*, 2020, **30**, 101468.
9 Q. Wang, Z. G. Qu, Z. Y. Jiang and W. W. Yang, *Appl. Energy*, 2018, **220**, 106–116.
10 N. Gurieff, C. Y. Cheung, V. Timchenko and C. Menictas, *J. Energy Storage*, 2019, **22**, 219–227.
11 Q. Zheng, F. Xing, X. Li, T. Liu, Q. Lai, G. Ning and H. Zhang, *J. Power Sources*, 2015, **277**, 104–109.
12 M. Yue, Q. Zheng, F. Xing, H. Zhang, X. Li and X. Ma, *AlChE J.*, 2018, **64**, 782–795.
13 K.-Q. Zhu, Q. Ding, J.-H. Xu, Y.-R. Yang, C. Yang, J. Zhang, Y. Zhang, T.-M. Huang, W.-M. Yan, Z.-M. Wan and X.-D. Wang, *Energy Convers. Manage.*, 2022, **267**, 115915.
14 E. Ali, H. Kwon, J. Choi, J. Lee, J. Kim and H. Park, *J. Energy Storage*, 2020, **28**, 101208.
15 H. Hao, Q.-A. Zhang, Z. Feng and A. Tang, *Chem. Eng. J.*, 2022, **450**, 138170.
16 R. Banerjee, N. Bevilacqua, L. Eifert and R. Zeis, *J. Energy Storage*, 2019, **21**, 163–171.
17 S. Kumar and S. Jayanti, *J. Power Sources*, 2016, **307**, 782–787.
18 V. Muñoz-Perales, M. van der Heijden, V. de Haas, J. Olinga, M. Vera and A. Forner-Cuenca, *ChemElectroChem*, 2024, **11**, e202300380.
19 J. Kim and H. Park, *J. Power Sources*, 2022, **545**, 231904.
20 Z. Guo, J. Sun, S. Wan, Z. Wang, J. Ren, L. Pan, L. Wei, X. Fan and T. Zhao, *Appl. Energy*, 2025, **379**, 124910.
21 Y. Jiang, M. Du, G. Cheng, P. Gao, T. Dong, J. Zhou, X. Feng, Z. He, Y. Li, L. Dai, W. Meng and L. Wang, *J. Energy Chem.*, 2021, **59**, 706–714.
22 Z. He, Y. Lv, T. Zhang, Y. Zhu, L. Dai, S. Yao, W. Zhu and L. Wang, *Chem. Eng. J.*, 2022, **427**, 131680.
23 K. Zhang, C. Yan and A. Tang, *J. Mater. Chem. A*, 2021, **9**, 17300–17310.
24 L. Qiao, M. Fang, J. Guo and X. Ma, *ChemElectroChem*, 2022, **9**, e202200292.
25 Y.-C. Chang, J.-Y. Chen, D. M. Kabtamu, G.-Y. Lin, N.-Y. Hsu, Y.-S. Chou, H.-J. Wei and C.-H. Wang, *J. Power Sources*, 2017, **364**, 1–8.
26 H. R. Jiang, W. Shyy, L. Zeng, R. H. Zhang and T. S. Zhao, *J. Mater. Chem. A*, 2018, **6**, 13244–13253.
27 Y. Huang, Q. Deng, X. Wu and S. Wang, *Int. J. Hydrogen Energy*, 2017, **42**, 7177–7185.
28 M. E. Lee, D. Jang, S. Lee, J. Yoo, J. Choi, H.-J. Jin, S. Lee and S. Y. Cho, *Appl. Surf. Sci.*, 2021, **567**, 150810.
29 H. Kim, J. S. Yi and D. Lee, *ACS Appl. Energy Mater.*, 2021, **4**, 425–433.
30 Z. Jialin, L. Yiyang, L. Shanfu and X. Yan, *Batteries*, 2023, **9**, 40.
31 Y. Jiang, Y. Wang, G. Cheng, Y. Li, L. Dai, J. Zhu, W. Meng, J. Xi, L. Wang and Z. He, *Carbon Energy*, 2024, **6**, e537.
32 M. Park, I.-Y. Jeon, J. Ryu, H. Jang, J.-B. Back and J. Cho, *Nano Energy*, 2016, **26**, 233–240.
33 T. Liu, X. Li, C. Xu and H. Zhang, *ACS Appl. Mater. Interfaces*, 2017, **9**, 4626–4633.
34 Q. Wu, X. Zhang, Y. Lv, L. Lin, Y. Liu and X. Zhou, *J. Mater. Chem. A*, 2018, **6**, 20347–20355.
35 J. Feng, Q. Guo, H. Liu, D. Chen, Z. Tian, F. Xia, S. Ma, L. Yu and L. Dong, *Carbon*, 2019, **155**, 491–498.
36 X. Du, J. Huang, J. Zhang, Y. Yan, C. Wu, Y. Hu, C. Yan, T. Lei, W. Chen, C. Fan and J. Xiong, *Angew. Chem., Int. Ed.*, 2019, **58**, 4484–4502.
37 H. Xu, J. Yang, R. Ge, J. Zhang, Y. Li, M. Zhu, L. Dai, S. Li and W. Li, *J. Energy Chem.*, 2022, **71**, 234–265.
38 K. Xie, X. Liu, H. Li, L. Fang, K. Xia, D. Yang, Y. Zou and X. Zhang, *Carbon Energy*, 2024, **6**, e427.
39 H. Radinger, A. Ghamlouche, H. Ehrenberg and F. Scheiba, *J. Mater. Chem. A*, 2021, **9**, 18280–18293.
40 R. M. Bachman, D. M. Hall and L. R. Radovic, *Carbon*, 2023, **201**, 891–899.
41 S. McArdle, H. Fiedler, J. Leveneur, J. Kennedy and A. T. Marshall, *J. Power Sources*, 2024, **608**, 234614.
42 S.-C. Kim, J. Paick, J. S. Yi and D. Lee, *J. Power Sources*, 2022, **520**, 230813.
43 S. J. Park, M. J. Hong, Y. J. Ha, J.-I. Choi and K. J. Kim, *Sci. Technol. Adv. Mater.*, 2024, **25**, 2327274.
44 Y. Gao, S. Zhang, X. Li, L. Li, L. Bao, N. Zhang, J. Peng and X. Li, *Carbon*, 2021, **181**, 323–334.
45 W. Gao, Z. Lin, H. Chen, S. Yan, Y. Huang, X. Hu and S. Zhang, *Fuel Process. Technol.*, 2022, **237**, 107468.
46 G. Ma, G. Ning and Q. Wei, *Carbon*, 2022, **195**, 328–340.
47 X. Cheng, F. Ran, Y. Huang, R. Zheng, H. Yu, J. Shu, Y. Xie and Y.-B. He, *Adv. Funct. Mater.*, 2021, **31**, 2100311.
48 A. B. Shah, Y. Wu and Y. L. Joo, *Electrochim. Acta*, 2019, **297**, 905–915.
49 H. Song, J. Yu, Z. Tang, B. Yang and S. Lu, *Adv. Energy Mater.*, 2022, **12**, 2102573.
50 E. Kano, J. Uzuhashi, K. Kobayashi, K. Ishikawa, K. Sawabe, T. Narita, K. Sierakowski, M. Bockowski, T. Ohkubo, T. Kachi and N. Ikarashi, *Phys. Status Solidi RRL*, 2024, **18**, 2400074.
51 S. Küspert, I. E. Campbell, Z. Zeng, S. E. Balaghi, N. Ortlieb, R. Thomann, M. Knäbbeler-Buß, C. S. Allen, S. E. Mohney and A. Fischer, *Small*, 2024, 2311260.
52 K. J. Kim, M.-S. Park, Y.-J. Kim, J. H. Kim, S. X. Dou and M. Skyllas-Kazacos, *J. Mater. Chem. A*, 2015, **3**, 16913–16933.
53 H. Hu, M. Yan, J. Jiang, A. Huang, S. Cai, L. Lan, K. Ye, D. Chen, K. Tang, Q. Zuo, Y. Zeng, W. Tang, J. Fu, C. Jiang,

Y. Wang, Z. Yan, X. He, L. Qiao and Y. Zhao, *Sci. Total Environ.*, 2024, **912**, 169141.
54 P. Wang, Y. Zhao, Y. Ban and M. Zheng, *J. Energy Storage*, 2024, **97**, 112859.
55 G. Nagarjuna, J. Hui, K. J. Cheng, T. Lichtenstein, M. Shen, J. S. Moore and J. Rodríguez-López, *J. Am. Chem. Soc.*, 2014, **136**, 16309–16316.
56 C. Wang, X. Li, X. Xi, W. Zhou, Q. Lai and H. Zhang, *Nano Energy*, 2016, **21**, 217–227.
57 M. Jing, Z. Xu, D. Fang, X. Fan, J. Liu and C. Yan, *J. Electrochem. Soc.*, 2021, **168**, 030539.
58 A. Duda, Z. Koza and M. Matyka, *Phys. Rev. E: Stat., Nonlinear, Soft Matter Phys.*, 2011, **84**, 036319.
59 M. Wang, J. Du, J. Zhou, C. Ma, L. Bao, X. Li and X. Li, *J. Power Sources*, 2019, **424**, 27–34.
60 S. Song, Y. Liang, Z. Li, Y. Wang, R. Fu, D. Wu and P. Tsiakaras, *Appl. Catal., B*, 2010, **98**, 132–137.
61 R. Jervis, M. D. R. Kok, T. P. Neville, Q. Meyer, L. D. Brown, F. Iacoviello, J. T. Gostick, D. J. L. Brett and P. R. Shearing, *J. Energy Chem.*, 2018, **27**, 1353–1361.
62 S. J. Yoon, S. Kim and D. K. Kim, *Energy*, 2019, **172**, 26–35.
63 H. R. Jiang, W. Shyy, M. C. Wu, R. H. Zhang and T. S. Zhao, *Appl. Energy*, 2019, **233–234**, 105–113.
64 A. Bayaguud, Y. Fu and C. Zhu, *J. Energy Chem.*, 2022, **64**, 246–262.
65 Z. Yang, T. Xu, H. Li, M. She, J. Chen, Z. Wang, S. Zhang and J. Li, *Chem. Rev.*, 2023, **123**, 11047–11136.
66 N. Mohamed and N. K. Allam, *RSC Adv.*, 2020, **10**, 21662–21685.
67 J. A. Teprovich, Jr., J. A. Weeks, P. A. Ward, S. C. Tinkey, C. Huang, J. Zhou, R. Zidan and P. Jena, *ACS Appl. Energy Mater.*, 2019, **2**, 6453–6460.
68 F. A. El Diwany, B. A. Ali, E. N. El Sawy and N. K. Allam, *Chem. Commun.*, 2020, **56**, 7569–7572.
69 Y. Zhou, L. Liu, Y. Shen, L. Wu, L. Yu, F. Liang and J. Xi, *Chem. Commun.*, 2017, **53**, 7565–7568.
70 M. U. Arshad, C. Wei, Y. Li, J. Li, M. Khakzad, C. Guo, C. Wu and M. Naraghi, *Carbon*, 2023, **204**, 162–190.
71 K. Zhang, H. Wang, X. Zhang, L. Liu, B. Feng, Y. Wang and J. Liu, *ACS Sustainable Chem. Eng.*, 2024, **12**, 7318–7328.
72 L. Dai, Y. Jiang, W. Meng, H. Zhou, L. Wang and Z. He, *Appl. Surf. Sci.*, 2017, **401**, 106–113.
73 C. Noh, B. W. Kwon, Y. Chung and Y. Kwon, *J. Power Sources*, 2018, **406**, 26–34.
74 Z. He, Y. Jiang, Y. Li, L. Wang and L. Dai, *Int. J. Energy Res.*, 2018, **42**, 1625–1634.
75 Y. Chung, C. Noh and Y. Kwon, *J. Power Sources*, 2019, **438**, 227063.
76 Z. He, G. Cheng, Y. Jiang, L. Wang and L. Dai, *J. Electrochem. Soc.*, 2018, **165**, A932.
77 L. Liu, X. Zhang, D. Zhang, K. Zhang, S. Hou, S. Wang, Y. Zhang, H. Peng, J. Liu and C. Yan, *Chem. Eng. J.*, 2023, **473**, 145454.
78 Q. Jiang, Y. Ren, Y. Yang, L. Wang, L. Dai and Z. He, *Composites, Part B*, 2022, **242**, 110094.
79 H. Yang, C. Fan and Q. Zhu, *J. Energy Chem.*, 2018, **27**, 451–454.
80 Y. Jiang, G. Cheng, Y. Li, Z. He, J. Zhu, W. Meng, H. Zhou, L. Dai and L. Wang, *Appl. Surf. Sci.*, 2020, **525**, 146453.
81 J. Sun, M. C. Wu, X. Z. Fan, Y. H. Wan, C. Y. H. Chao and T. S. Zhao, *Energy Storage Mater.*, 2021, **43**, 30–41.
82 X. Zhang, Q. Wu, Y. Lv, Y. Li and X. Zhou, *J. Mater. Chem. A*, 2019, **7**, 25132–25141.
83 Z. Xu, M. Jing, J. Liu, C. Yan and X. Fan, *J. Mater. Sci. Technol.*, 2023, **136**, 32–42.
84 C. Pan, C. Wang, Y. Fang, Y. Zhu, H. Deng and Y. Guo, *Environ. Sci.: Nano*, 2021, **8**, 1863–1885.
85 Y. Ren, F. Yu, X.-G. Li and J. Ma, *Mater. Today Chem.*, 2021, **22**, 100603.
86 L. Xia, Q. Zhang, C. Wu, Y. Liu, M. Ding, J. Ye, Y. Cheng and C. Jia, *Surf. Coat. Technol.*, 2019, **358**, 153–158.
87 H. Fu, X. Bao, M. He, J. Xu, Z. Miao, M. Ding, J. Liu and C. Jia, *J. Power Sources*, 2023, **556**, 232443.
88 Q. Li, J. Liu, A. Bai, P. Li, J. Li, X. Zhang, M. Yu, J. Wang and H. Sun, *J. Chem.*, 2019, **2019**, 1–9.
89 T. Long, Y. Long, M. Ding, Z. Xu, J. Xu, Y. Zhang, M. Bai, Q. Sun, G. Chen and C. Jia, *Nano Res.*, 2021, **14**, 3538–3544.
90 J. L. Suter, R. C. Sinclair and P. V. Coveney, *Adv. Mater.*, 2020, **32**, 2003213.
91 J. Li, B. Ji, R. Jiang, P. Zhang, N. Chen, G. Zhang and L. Qu, *Carbon*, 2018, **129**, 95–103.
92 D. O. Opar, R. Nankya, J. Lee and H. Jung, *Appl. Surf. Sci.*, 2020, **531**, 147391.
93 J. Guo, L. Pan, J. Sun, D. Wei, Q. Dai, J. Xu, Q. Li, M. Han, L. Wei and T. Zhao, *Adv. Energy Mater.*, 2024, **14**, 2302521.
94 M. Park, Y.-j Jung, J. Kim, H. i Lee and J. Cho, *Nano Lett.*, 2013, **13**, 4833–4839.
95 Y. Zhang, Q. Wan and N. Yang, *Small*, 2019, **15**, 1903780.
96 J. Zhu, A. Holmen and D. Chen, *ChemCatChem*, 2013, **5**, 378–401.
97 M. Faraji and M. Mohseni, *Ionics*, 2018, **24**, 2753–2760.
98 P. Han, Y. Yue, Z. Liu, W. Xu, L. Zhang, H. Xu, S. Dong and G. Cui, *Energy Environ. Sci.*, 2011, **4**, 4710–4717.
99 L. Ye, S. Qi, T. Cheng, Y. Jiang, Z. Feng, M. Wang, Y. Liu, L. Dai, L. Wang and Z. He, *ACS Nano*, 2024, **18**, 18852–18869.
100 Y. Chen, H. Fu, W. Yang, L. Zhong, Q. Wang, B. Lu, N. Wang, Z. Chen, G. Shi, C. Jia, M. Ding, R. Xia, E. I. Iwuoha, U. Feleni, S. Admassie and X. Peng, *ACS Sustainable Chem. Eng.*, 2024, **12**, 10567–10576.
101 Z. Hu, Z. Miao, Z. Xu, X. Zhu, F. Zhong, M. Ding, J. Wang, X. Xie, C. Jia and J. Liu, *Chem. Eng. J.*, 2022, **450**, 138377.
102 B. Huang, Y. Liu, M. Xia, J. Qiu and Z. Xie, *Sustainable Energy Fuels*, 2020, **4**, 559–570.
103 K. Amini, J. Gostick and M. D. Pritzker, *Adv. Funct. Mater.*, 2020, **30**, 1910564.
104 M. H. Hossain, N. Abdullah, K. H. Tan, R. Saidur, M. A. Mohd Radzi and S. Shafie, *The Chem. Record*, 2024, **24**, e202300092.
105 R. Zhang, K. Li, S. Ren, J. Chen, X. Feng, Y. Jiang, Z. He, L. Dai and L. Wang, *Appl. Surf. Sci.*, 2020, **526**, 146685.
106 Z. Yu, X. Jia, H. Gao, R. Su, X. Wang, T. Zhao and H. Jiang, *Adv. Funct. Mater.*, 2024, 2420534.

107 T. Liu, X. Li, H. Nie, C. Xu and H. Zhang, *J. Power Sources*, 2015, **286**, 73–81.
108 D. J. Suárez, Z. González, C. Blanco, M. Granda, R. Menéndez and R. Santamaría, *ChemSusChem*, 2014, **7**, 914–918.
109 Y. Wen, T. P. Neville, A. Jorge Sobrido, P. R. Shearing, D. J. L. Brett and R. Jervis, *J. Power Sources*, 2023, **566**, 232861.
110 B. Li, M. Gu, Z. Nie, Y. Shao, Q. Luo, X. Wei, X. Li, J. Xiao, C. Wang, V. Sprenkle and W. Wang, *Nano Lett.*, 2013, **13**, 1330–1335.
111 X. Yang, T. Liu, C. Xu, H. Zhang, X. Li and H. Zhang, *J. Energy Chem.*, 2017, **26**, 1–7.
112 H. R. Jiang, Y. K. Zeng, M. C. Wu, W. Shyy and T. S. Zhao, *Appl. Energy*, 2019, **240**, 226–235.
113 L. Liu and A. Corma, *Chem. Rev.*, 2018, **118**, 4981–5079.
114 X. Zhou, X. Zhang, L. Mo, X. Zhou and Q. Wu, *Small*, 2020, **16**, 1907333.
115 X. Liu, Y. Nie, L. Yu, L. Liu and J. Xi, *J. Energy Storage*, 2024, **91**, 112035.
116 F. Xing, Q. Fu, F. Xing, J. Zhao, H. Long, T. Liu and X. Li, *J. Am. Chem. Soc.*, 2024, **146**, 26024–26033.
117 S. Mehboob, A. Mehmood, J.-Y. Lee, H.-J. Shin, J. Hwang, S. Abbas and H. Y. Ha, *J. Mater. Chem. A*, 2017, **5**, 17388–17400.
118 J. Shen, S. Liu, Z. He and L. Shi, *Electrochim. Acta*, 2015, **151**, 297–305.
119 D. Cheng, Y. Li, C. Han, Z. He, J. Zhu, L. Dai, W. Meng and L. Wang, *Colloids Surf., A*, 2020, **586**, 124137.
120 J. Xu, Y. Zhang, Z. Huang, C. Jia and S. Wang, *Energy Fuels*, 2021, **35**, 8617–8633.
121 J. Vázquez-Galván, C. Flox, C. Fàbrega, E. Ventosa, A. Parra, T. Andreu and J. R. Morante, *ChemSusChem*, 2017, **10**, 2089–2098.
122 N. Yun, J. J. Park, O. O. Park, K. B. Lee and J. H. Yang, *Electrochim. Acta*, 2018, **278**, 226–235.
123 H. Zhou, J. Xi, Z. Li, Z. Zhang, L. Yu, L. Liu, X. Qiu and L. Chen, *RSC Adv.*, 2014, **4**, 61912–61918.
124 Y.-S. Hsiao, J.-H. Huang, H.-Y. Lin, W. K. Pang, M.-T. Hung, T.-H. Cheng, S.-C. Hsu, H. C. Weng and Y.-C. Huang, *Surf. Coat. Technol.*, 2024, **484**, 130785.
125 M. G. Hosseini, S. Mousavihashemi, S. Murcia-López, C. Flox, T. Andreu and J. R. Morante, *Carbon*, 2018, **136**, 444–453.
126 X. Wu, H. Xu, L. Lu, H. Zhao, J. Fu, Y. Shen, P. Xu and Y. Dong, *J. Power Sources*, 2014, **250**, 274–278.
127 X. Xie, Y. Xiang and W. A. Daoud, *ACS Appl. Energy Mater.*, 2020, **3**, 10463–10476.
128 X. Huang, K. Zhang, B. Peng, G. Wang, M. Muhler and F. Wang, *ACS Catal.*, 2021, **11**, 9618–9678.
129 A. W. Bayeh, G.-Y. Lin, Y.-C. Chang, D. M. Kabtamu, G.-C. Chen, H.-Y. Chen, K.-C. Wang, Y.-M. Wang, T.-C. Chiang, H.-C. Huang and C.-H. Wang, *ACS Sustainable Chem. Eng.*, 2020, **8**, 16757–16765.
130 F. Chen, X. Cheng, L. Liu, L. Han, J. Liu, H. Chen, Q. Zhang and C. Yan, *J. Power Sources*, 2023, **580**, 233421.
131 Y. Jiang, G. Cheng, Y. Li, Z. He, J. Zhu, W. Meng, L. Dai and L. Wang, *Chem. Eng. J.*, 2021, **415**, 129014.
132 D. Wang, Z. Lin, T. Wang, Z. Yao, M. Qin, S. Zheng and W. Lu, *J. Hazard. Mater.*, 2016, **308**, 328–334.
133 Y. Lv, C. Han, Y. Zhu, T. Zhang, S. Yao, Z. He, L. Dai and L. Wang, *J. Mater. Sci. Technol.*, 2021, **75**, 96–109.
134 L. Wei, T. Zhao, L. Zeng, X. Zhou and Y. Zeng, *Energy Technol.*, 2016, **4**, 990–996.
135 L. Wei, L. Zeng, M. S. Han, W. J. Li, L. P. Chen, J. H. Xu and T. S. Zhao, *J. Power Sources*, 2023, **576**, 233180.
136 G. Cheng, Y. Jiang, Y. Li, J. Chen, Z. He, W. Meng, L. Dai and L. Wang, *Electrochim. Acta*, 2020, **362**, 137178.
137 A. W. Bayeh, D. M. Kabtamu, Y.-T. Ou, N.-Y. Hsu, H.-H. Ku, Y.-M. Wang, T.-C. Chiang, H.-C. Huang and C.-H. Wang, *ACS Sustainable Chem. Eng.*, 2022, **10**, 12271–12278.
138 H. R. Jiang, W. Shyy, M. C. Wu, L. Wei and T. S. Zhao, *J. Power Sources*, 2017, **365**, 34–42.
139 Y. Huang, J. Huo, S. Dou, K. Hu and S. Wang, *RSC Adv.*, 2016, **6**, 66368–66372.
140 R. Huang, S. Liu, Z. He, W. Zhu, G. Ye, Y. Su, W. Deng and J. Wang, *Adv. Funct. Mater.*, 2022, **32**, 2111661.
141 Z. Huang, Z. Chen, M. Yang, M. Chu, Z. Li, S. Deng, L. He, L. Jin, R. E. Dunin-Borkowski, R. Wang, J. Wang, T. Yang and Y. Xiao, *Energy Environ. Sci.*, 2024, **17**, 5876–5891.
142 X. He, J. M. Larson, H. A. Bechtel and R. Kostecki, *Nat. Commun.*, 2022, **13**, 1398.